Investigations of the Dynamical Evolution of Lunar Ejecta

by

Logan Fladeland

B.Sc., Combined Honours Physics and Astronomy, The University of British Columbia, 2019

A THESIS SUBMITTED IN PARTIAL FULFILLMENT
OF THE REQUIREMENTS FOR THE DEGREE OF

Master of Science

in

THE FACULTY OF GRADUATE AND POSTDOCTORAL STUDIES
(Astronomy)

The University of British Columbia
(Vancouver)

October 2022

The following individuals certify that they have read, and recommend to the Faculty of Graduate and Postdoctoral Studies for acceptance, the thesis entitled:

Investigations of the Dynamical Evolution of Lunar Ejecta

submitted by **Logan Fladeland** in partial fulfillment of the requirements for the degree of **Master of Science** in **Astronomy**.

Examining Committee:

Aaron Boley, UBC Physics and Astronomy
Supervisor

J.J. Kavelaars, NRC Canada and UBC Physics and Astronomy
Supervisory Committee Member

Abstract

Humanity is on course to return to the surface of the Moon within the next decade, with plans and aspirations of permanently crewed stations that could eventually become self-sustained through advancements of in-situ resource utilization (ISRU). During NASA's Apollo era, which saw the first and only humans step foot on the Moon, the issue of lunar dust rose to prominence as it was found to be quite abrasive and became coated on practically every type of material. Natural mechanisms have been discovered that can levitate lunar dust and soil above the surface, at times creating a faint haze around the Moon. Increasing lunar surface activity, including potential construction and mining operations, as well as a significant increase in landings and departures, could see large amounts of material artificially jettisoned, if proper mitigation techniques are not introduced. N-body simulations of 10,000 particles ejected from the Moon are performed using REBOUND to examine some of the different dynamical pathways available to material escaping the low lunar gravity. Particles that do not collide with the Moon or the Earth generally end up in orbit around the Earth or escape onto heliocentric orbits, with very few left orbiting the Moon after one year. A constant delivery of particles to the L1 and L2 Earth-Moon Lagrange points is seen, with sporadic activity at the three other Lagrange points. Moreover, the possibility of long-lived dust in the cis-lunar environment raises questions about how lunar activities will impact the night sky. To that end, the particles are projected onto the sky for an observer on Earth and the associated brightness is calculated.

Lay Summary

Multiple ongoing efforts to return humans to the Moon and establish long-term operations present a need to better understand the transport and evolution of dust and meteoroids throughout the Earth-Moon environment. This study investigates such evolution by running dynamics simulations of ejected particles from the Moon's surface to analyze the short and long-term behavior of such material. The accumulation of material in locations of potential future lunar operations is studied, along with statistics of collisions with the Earth or Moon, as well as the number of particles escaping onto orbits about the Sun. Projections of the night sky from Earth allow for estimations of the brightness of reflected sunlight arriving from these particles. Further applications of this work can help determine potential limits on the amount of material allowed to escape the lunar surface in order to avoid impacting spacecraft operations or increasing the brightness of the night sky.

Preface

The content of this thesis is original unpublished work by the author. The idea for this study came about through discussions with the author's supervisor, Dr. Aaron Boley. All necessary python scripts, as well as the resulting plots and data were created by the author. Individual techniques and methods used but not developed by the author have been cited where appropriate.

Table of Contents

List of Figures

Glossary

ILRS International Lunar Research Station

NASA National Aeronautics and Space Administration

LEO Low Earth Orbit

CSM Command and Service Module

LM Lunar Module

EVA Extravehicular Activity

ISS International Space Station

ESA European Space Agency

SLS Space Launch System

NRHO Near-Rectilinear Halo Orbit

CR3BP Circular Restricted Three Body Problem

ISRU In-Situ Resoure Utilization

Chapter 1

Introduction

Humanity is renewing its effort to return to the Moon with plans to develop long-term human habitation on the Moon's surface and in cis-lunar space. Moreover, a larger range of actors are seeking to take part in possible lunar development, including national space agencies and private enterprises. Uses of the Moon are envisaged to include scientific sampling, lunar-based observations, space resource processing for exploration and energy needs, and even tourism [9, 28]. While many benefits are expected to be derived from this expansion into space, we must be mindful of any unintended and potentially harmful consequences of our actions. As we begin to create a long-term presence on the Moon, it's important we do so in a way that is as sustainable as possible, to allow future generations to continue to explore and enjoy the wonders and beauty of our celestial companion.

Two major multinational groups are emerging in this return to the Moon, with the United States led Artemis program forming concurrently as China and Russia develop plans for their own jointly led international lunar base. The Artemis Accords, signed by 22 countries and territories[1], seeks to build upon the limited international framework surrounding the uses of outer space, while supporting and promoting peaceful activities and best practices for space exploration. Several signatories of the Accords, working together with private companies, are seeking to return to the surface of the Moon by the mid 2020s, with plans of eventually build-

[1]As of July 14, 2022. The Accords can be accessed at: https://www.nasa.gov/specials/artemis-accords/img/Artemis-Accords-signed-13Oct2020.pdf

ing a long-term base previously referred to as the Artemis Base Camp [28]. Meanwhile, China and Russia are developing plans to build the International Lunar Research Station (ILRS), with construction expected to begin before the end of the 2020s, however it is currently not expected to be crewed until about a decade after construction begins [9]. While the two groups are promoting peace and cooperation, with both open to new nations joining them, it does not appear that the two groups are looking to work together any time soon. The co-emergence of the two groups may push each other to exciting new advancements, but with the prospects of emerging economic opportunities, combined with the competitiveness of human nature, we must be cautious as we proceed. As such, it may be worth examining the last time the US and Russia (formerly USSR) engaged in such a race.

During the late 1950s and early 1960s, amid the tense Cold War, the Soviet Union and the United States become the first nations to achieve spaceflight, with their rivalry pushing each other to greater and greater heights. In 1957, the USSR successfully launched the first artificial satellite (Sputnik 1) into orbit around the Earth, signifying the beginning of the space race. Just two years later, the Soviets were already conducting several lunar missions, including the first fly-by of the Moon (Luna 1), the first spacecraft to impact the surface of the Moon (Luna 2), and successfully capturing and sending back to Earth the first images of the far side of the Moon (Luna 3). While the US were also making significant strides matching the achievements of the Soviets, it seemed that the USSR was often just a few months ahead, with several notable firsts, including the first animal in orbit (Sputnik 2)[2]. By 1961, just four years after Sputnik 1 was launched, both the USSR and the US would successfully complete human spaceflight missions, though the Soviets would again just beat the Americans, this time by less than a month. Following these crewed missions, former U.S. President John F. Kennedy delivered his now famous address to Congress, calling for America to land a man on the Moon and return him to Earth by the end of the 1960s. Although the former President did not explicitly say in this speech that the US needed to land a man on the Moon

[2]This was a stray dog named Laika. While Sputnik 2 was able to successfully make it to orbit, Laika ultimately passed away reportedly due to overheating caused by a broken air conditioning. Additionally, prior to launch it was fully understood she would not survive the entire mission [6], so, personally, I find it difficult to characterize the mission as a success. Nevertheless, she provided valuable information about living organisms in spaceflight.

before the Soviets, it was quite clear that doing so would ultimately determine if the mission was a complete success or not. This address set the foundations for NASA's Apollo program, which would attempt to deliver on JFK's bold ambitions and, as a result, win the Space Race.

As the two competing space superpowers charted their journeys to the Moon, neither had much of an idea about what they were getting into, as very little was known about the Moon prior to the Apollo era. Regardless of the sheer magnitude of technological innovations that would be required to make it there, it was unknown exactly what the surface would be like and how extreme the radiation would be. In 1955, Gold [15] theorized that impacts and the intense lunar radiation environment would eventually erode the lunar surface into a fine dust. While this theory would help explain why the Moon had such a surprisingly low albedo, Gold was unable to estimate the thickness of the dust layer as the speed of this erosion was dependent on factors still uncertain at the time [4]. This created some fears that the Moon could have a deep layer of dust covering the surface that would cause heavy spacecraft to sink, potentially preventing any safe landing attempts.

Several more missions in the mid 1960s by both countries would give the two valuable insight and help answer some of the unknowns about the Moon at the time, while also highlighting the perils of the task ahead. The USSR would continue its record of significant milestones, including the first successful soft landing of a spacecraft on the Moon with its Luna 9 mission in 1966. Importantly, Luna 9 confirmed that the surface of the Moon could support a lander and that it would not sink into the ground, although Gold [15] was correct as the surface was indeed covered in dust [37]. Just as before though, the US was not far behind as four months later, the American Surveyor 1 was also able to safely land on the surface of the Moon. Impressively however, the Surveyor 1 mission was successful on the first soft landing attempted by the US, while the Soviet Union had several failed attempts in the years prior, including Luna 4, 5, 6, 7, and 8. Following a multi-year test campaign of the new Saturn family of rockets and the success of Surveyor 1, the US would look to attempt its first crewed flight of the Apollo era in February of 1967 with Apollo 1. Unfortunately, the crew members would never get the chance to lift-off, as all three tragically died in a fire during testing on the launch pad less than one month prior to their expected launch. This would ultimately lead to a

20-month hiatus in attempted crewed flights for the Apollo program.

Following this tragic start to Apollo, NASA continued their uncrewed operations as the rest of 1967 saw them launch 8 lunar missions, including the Surveyor 5 lander, which provided an unanticipated discovery. Images taken from the surface of the Moon as the Sun was setting below the horizon revealed a haze extending away from the Moon. This haze indicated that the sunlight was being scattered, similar to what happens on Earth due to its atmosphere, but the Moon's atmosphere is practically non-existent. What Surveyor 5 had discovered was lunar dust floating above the surface that is capable of creating a similar effect, which was further confirmed by follow up images from Surveyor 6 and 7, shown in Figure 1.1 [31]. Although unexpected, the idea had been brought forward before by Gold [15], who originally theorized the lunar surface was covered in a layer of dust, as he predicted

Figure 1.1: Surveyor 6 image of a sunset seen from the surface of the Moon [3]. A haze can be seen, indicating the light is getting scattered. Credit: NASA

the same mechanism that forms the dust could be capable of dispersing it up off the surface [4]. At the time, it was still unclear entirely what the source of the dust was, but the amount observed was not enough to give pause to any future missions.

Several more significant missions followed that would give the two nations confidence that a crewed lunar landing could be done, and potentially still within this decade. In September 1968, the Soviets Zond 5 spacecraft completed the first mission to fly around the moon with animals onboard and return them to Earth safely, and less than 1 month later, the Apollo crewed program was ready to make a return. A successful launch saw the Apollo 7 crew spend 10 days and complete over 160 orbits in low Earth orbit (LEO)[3]. The crewed Apollo 8 would launch just two months later, surpassing the achievements of the Soviets Zond 5 by successfully achieving the first humans in orbit about the Moon, capturing the iconic 'Earthrise' photo in the process, shown in Figure 1.2. With JFK's deadline to land on the Moon before the end of the decade quickly approaching, 1969 would see a number of historic missions launched for the Apollo program. In accordance with their newly condensed launch timeline, Apollo 9 was ready to launch in March, just three months after Apollo 8. It was the first mission to contain and successfully demonstrate the capabilities of both the Command and Service Module (CSM) and the Lunar Module (LM). Apollo 10 would launch just two months later, serving as a dress rehearsal for an actual landing attempt, and following this successful test, NASA was confident it could attempt a crewed Moon landing.

Launching atop a Saturn V rocket on July 16th, 1969, two months after the most recent Apollo mission, 29 months after the fatal Apollo 1 disaster, and eight years after JFK's proclamation, Apollo 11 set out on course to the Moon to attempt the first crewed lunar landing. Four days into the mission, Neil Armstrong and Buzz Aldrin piloted their LM 'Eagle' to a successful landing on the Moon. During their stay, they collected soil and rock samples, took photos and videos, and deployed instruments including a retroreflector for lunar ranging and a seismic device for measuring moonquakes [43]. After almost a full day on the surface, including over two hours of extravehicular activities (EVAs), Eagle ascended to rejoin the CSM 'Columbia' and set out back for Earth with over 20 kg of lunar rocks

[3]LEO is often defined as orbits contained within 2000 km of the Earth's surface, but generally are just a few hundred kilometers in altitude. For reference, the Moon is almost 400,000 km away.

Figure 1.2: Image of the Earth taken by Apollo 8 astronauts as it rose from behind the Moon while the crew was in orbit about the Moon. Credit: NASA

and soil [46]. The Apollo 11 crew safely returned to Earth after being in space for over eight days, achieving JFK's goal just five months before the end of the decade, and in doing so, beating the Soviets to the Moon, and effectively declaring themselves as the winners of the space race.

NASA would go on to launch six additional crewed missions under the Apollo program, with the final, Apollo 17, launching in December of 1972. The entire Apollo program would see 12 different men plant their feet on the Moon, spending over one week combined on the surface, with almost half the time spent during EVAs and almost 400 kg (840 lbs) of lunar rocks and soil returned to Earth [46]. Apollo 17's Lunar Ejecta and Meteorites Experiment also provided additional evidence of the lunar dust floating above the surface of the Moon that was first observed by the Surveyor probes. Designed to detect lunar impacts and the subsequent ejecta, the resulting data was overwhelmed by dust from the Moon that was instead highly charged and slow moving, not what is expected for impact ejecta [1]. While these missions inspired generations and provided us with incredible knowledge and perspectives, the extreme dangers and costs of the program were hard to ignore.

Although initially denied publicly, the Soviets had simultaneously been developing a crewed lunar program of their own, attempting to mirror the Apollo program, but they would never attempt a crewed lunar landing. Their first crewed mission of the program (Soyuz 1), which launched just two months after the Apollo 1 tragedy, would again show the perils of spaceflight. After successfully launching to orbit, the solo-crewed mission quickly encountered a variety of issues, resulting in the spacecraft returning to Earth early. The lone cosmonaut would unfortunately not survive reentry, with this becoming the first in-flight fatality of a space mission. The Soviets were also developing a massive new rocket to take their crews to the moon, but four failed launch attempts of the N1 would see the rocket's development suspended, and ultimately canceled. These difficulties, paired with the success of the Apollo missions, would eventually dissolve Soviet ambitions of a crewed landing attempt [7]. While the Soviets would still beat the Americans to getting the first rover onto the surface of the Moon with the Lunokhod 1 mission, it would prove to be one of their last major space achievements regarding the Moon. The 1975 joint Apollo-Soyuz mission saw a historic first as the two 'rivals' docked their crewed spacecraft together in orbit, with a symbolic handshake arguably ending the space race and marking a new era of cooperation in space. At the time of this writing, the US remains the only country to have safely landed a crew on the Moon and returned them to Earth, with almost 50 years passing since the final trip was made.

During the Apollo Moon landings, one unforeseen issue that plagued the crews was the dust on the surface. Although the presence of the lunar dust was becoming widely accepted prior to the first missions, the number of different problems it created was not predicted [2, 12]. The troubles began immediately during their visit, as large amounts of material were kicked up during the landings, greatly decreasing visibility for the pilots [12, 42]. Once on the surface, the problems continued as the dust was found to stick to everything, covering their spacesuits and equipment, and when the astronauts tried to wipe it off their suits, they found it got rubbed deeper into the fabrics [8, 12]. Lunar regolith is created by the shattering of lunar bedrock from billions of years of impacts, and without the weathering that occurs on Earth, these particles can remain quite sharp and jagged [13]. This became a bigger problem still once the astronauts would return inside their lunar module, as the dust remained on their suits, with some getting kicked up into the air and becoming a lung and eye irritant [12, 42]. The full extent of the toxicological of lunar dust is still not fully understood to this day, and while no long-term problems for the astronauts were attributed to the dust, prolonged exposure could have adverse effects on astronauts' lungs, eyes, and skin [13, 18].

Despite rising concerns about how dust could impact crewed lunar missions, NASA was not deterred and performed several studies in the 1970s about the habitability of the Moon. During the early part of the decade, while still conducting Apollo missions, NASA was already studying lunar orbital stations and locations for surface bases [16, 17, 23]. One such proposal was a 24-person lunar surface base called MOONLAB. It would require 15 years and 37 Saturn V launches to build the base, and would have contained a farm for growing food, doubling as a CO_2 removal system [18]. Additionally, to support long-term lunar missions and habitats, several studies investigated the feasibility of mining the Moon. A variety of methods were proposed included using nuclear explosives [19] and drilling gas wells [35]. Methods of mining water on the Moon were also studied, at a time when it was still unknown if there was even water available [34]. Unfortunately for the lunar enthusiasts, while the issue of dust remained a constant throughout these studies, the political ambitions funding the lunar program were not. A recently elected US president no longer saw the risk of lunar missions necessary, as he thought a disaster could impact his re-election chances [22]. Gradually, the program was brought to an end as three planned Apollo missions were cancelled and funds got diverted towards NASA's new poster child, the Space Shuttle.

The decades following the Apollo era would see a relatively consistent human presence in space, although the crewed missions would remain within LEO, as lunar activity faded despite a strong interest in the Moon remaining. Several space stations were launched to LEO, notably the International Space Station (ISS), providing a safer, more accessible option than traveling to the Moon. While the 1980s would see no lunar missions launched by either the US or the Soviet Union, the

1990s would start with a new country launching a mission to the Moon. The Japanese Hiten spacecraft, launched in 1990, experienced some initial setbacks but was eventually able to successfully enter lunar orbit. The US would launch just two lunar missions that decade, with Clementine launched in 1994, and the Lunar Prospector in 1998. However, the 2000s would see a resurgence in activity and plans for lunar missions, with several new agencies joining in. The European Space Agency (ESA) would launch their first lunar orbiter, SMART-1, in 2003. This was followed shortly after by the Chinese Chang'e 1 in 2007 and India's Chandrayaan-1 the year after. As new countries were setting out to explore the Moon for the first time, America was finally making plans for a crewed return to the surface. In 2005, the NASA Constellation program was announced, with part of its goal being a crewed return to the Moon by 2020. This goal was not met, as since the program was announced, its priorities have shifted with the changing of presidents. The program was rebranded as Artemis in 2017, and the first crewed landing is now scheduled for 2025. Although its uncertain if this deadline will be met, it appears to be a question of when, rather than if, the mission will launch.

The Artemis program, as well as the agreements in place between China and Russia, are a sign that we are about to enter a new era of lunar exploration, this time with the intent to stay, permanently. Part of the objectives of the Artemis program is to build an outpost on the surface of the Moon that could be crewed for long-duration missions [28]. The ILRS, which is currently expected to begin construction around 2026, will seek to do the same [9]. The first test flight of the Space Launch System (SLS) rocket, which is being built to launch the Artemis crew, is scheduled for later this year (2022). Regardless of when the first launch of SLS takes place, the Artemis era has begun, as the first support mission has already been launched. CAPSTONE was launched in June of 2022 and is currently on its way[4] into a special lunar orbit called a near-rectilinear halo orbit (NRHO).

Figure 1.3 demonstrates what some NRHOs look like, seen from a side-on view of the Moon's rotational frame about the Earth. The NRHO family of orbits are a result of the circular restricted three body problem (CR3BP), which assumes one body is on a circular orbit around a more massive object, while the third body

[4] At the time of writing.

is required to have a negligible mass compared to the other two. This is a safe assumption here as the Earth and the Moon are both much more massive than any spacecraft and the Moon's orbit is approximately circular about the Earth for the purposes of this discussion. A consequence of the CR3BP is the five equilibrium positions in the rotating frame, known as the Lagrange points. Three of these points, known as the collinear points, lie along the x-axis of the rotating frame, while the other two, L4 and L5, are about 60° ahead and behind the Moon in orbit about the Earth. The two collinear points closest to the Moon are L1 and L2, with L1 located between the Earth and the Moon, and L2 beyond the far side of the Moon, shown in Figure 1.3. L3 is the final collinear point, located about one lunar distance away from the Earth in the opposite direction of the Moon. Halo orbits are

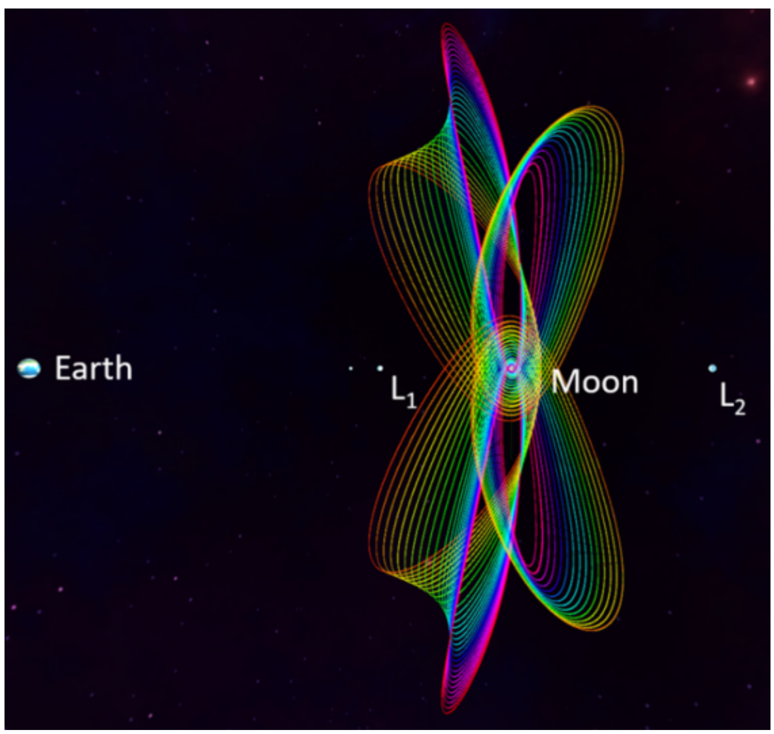

Figure 1.3: Examples of the northern and southern NRHOs about L1 and L2. The figure is shown from a side-on perspective of the Moon's rotational frame about the Earth. The Earth-Moon L1 and L2 Lagrange points are shown for reference. Credit: Davis et al. [11] (Used with Permission)

stable orbits that can form about the three collinear points. NRHOs are a subset of these halo orbits, and although the CR3BP is not exact for the Earth-Moon system, they are still relatively stable, so not a lot of energy would be required to keep a ship in such an orbit [21, 47].

CAPSTONE was launched to verify the stability of NRHOs, as NASA envisages using the same orbits eventually for the Lunar Gateway, which is planned to be the first space station to orbit the Moon. One benefit of these orbits is that the spacecraft will be able to maintain almost constant communication with the Earth, as it is designed to limit the Moon passing in between the spacecraft and the Earth [21, 47]. Another feature of a NRHO is that it has a very close approach to the Moon at periselene and such a distant aposelene that it sets an easy transfer point for Earth-Moon connections. Gateway will act as a transfer station in the southern L2 NRHO for missions to the lunar surface and beyond. Once the technology for in-situ resource utilization (ISRU)[5] becomes available, we could see Gateway serve as a fuel depot, enabling lunar landers to extend their mission lifetimes and refueling spacecraft bound for deep-space [21].

The new space race seeks to build human lunar habitats and increase surface activity on the Moon in general, with ISRU at its core, but we must be mindful to proceed in a sustainable manner if we want it to last. One issue we must be careful of as we return to the Moon is orbital debris, including discarded rocket stages and defunct satellites, as well as disturbed lunar soil that can get lofted into cis-lunar space. It should be clear by now that we cannot be allowed to underestimate our collective ability to pollute seemingly enormous bodies, as we've already proven with the Earth's oceans and waterways, atmosphere, and now orbital environment. Although nations have previously been extremely careful to avoid contaminating the lunar surface, common practice has also seen these same nations discard rocket stages by crashing them into the Moon (both intentionally and unintentionally). In addition to ejecta from natural and artificial impactors, landing and takeoff sequences on the lunar surface will eject a large amount of material, as experienced by the Apollo missions. Some particles will be able to reach escape velocities and

[5]ISRU is another way of saying space mining. Water ice, discovered in craters near the lunar south pole, is likely to be the target of the first mining operations, as water is not only an important resource for human survival, it can also be broken down and used as rocket fuel [32].

enter orbit, while buildings or equipment in the vicinity will also be prone to damage [20, 44]. Once on the surface of the Moon, the disturbances will only continue. The construction of infrastructure on the surface is likely to disrupt lots of soil, in addition to the inevitable emergence of ISRU and the mining of the lunar south pole for water ice [32]. Additionally, while private companies are currently focused on supporting national agencies, in a not-too-distant future, we could see a shift towards the commercialization of the Moon, with lunar hotels and resorts becoming a reality. If we are to move forward in a sustainable manner, it is important that we try to avoid making mistakes we've previously made while learning from our past.

Since humans last stepped foot on the Moon, we now know much more about our celestial companion and technology has vastly improved, but problems such as the lunar dust could still limit any progress. The dust first discovered extending beyond the lunar surface by the Surveyor program is now better understood. Electrostatic charges on the particles interacting with lunar surface charges caused by solar radiation and the lunar plasma environment can launch particles off the surface and allow them to levitate [10, 36, 40]. The majority of the charged particles that get lofted above the surface are on ballistic trajectories that will eventually return to the surface [40]. In addition to natural mechanisms, lunar soil can also get dispersed from the surface through anthropogenic processes. Some of this material could exceed escape speeds and ultimately get ejected out into the cis-lunar orbital environment. Escaping material could potentially build up in regions of high spacecraft activity, including the Earth-Moon Lagrange points. Understanding the behaviour of these particles, both those on suborbital ballistic trajectories, as well as the high-speed orbital ejecta, is important for our anticipated return to the Moon. Yang et al. [45] recently studied the distribution of dust that is ejected from the Moon, integrating a variety of particle sizes released from plausible ejection models for 100 years and analyzed the end state. Their simulations showed most particles escaped the Earth-Moon system by the end of the 100 years, with some particles found to collide with the Earth or the Moon.

One final consideration we should keep in mind when examining our possible impacts on the cis-lunar environment is the ability to alter the brightness of the night sky. Ejected lunar material can reflect sunlight, and a sufficient spatial density of material in orbit could produce brightness levels that exceed the background sky.

This idea is not necessarily new, as particles have been theorized to gather in the L4 and L5 Earth-Moon Lagrange points, referred to as the Kordylewski clouds[6]. These clouds have been imaged several times but are not bright enough to see with the naked eye [39]. The night sky is arguably common heritage of humankind, and as such, it should be protected. Human-caused changes to the sky could have a number of unintended consequences, including for science, as well as natural and cultural heritage. While studies on the impacts of lunar dust on the night sky brightness could not be found, one study discussed the negative impacts it could have on future astronomical observations attempted from the Moon [27].

As we proceed to return to the Moon, we should attempt to limit our impact on the natural lunar environment to the best of our ability. This includes preventing the buildup of any long-lasting orbital debris, including lunar soil disturbed from the surface. To address some of these issues, this study seeks to gain a better understanding of the dynamical behavior of lunar ejecta. Particles ejected from the Moon are simulated and tracked for one year to determine the short and longer-term behavior of the particles in the cis-lunar environment. The accumulation of material near the Earth-Moon Lagrange points is studied, as well as statistics regarding particle collisions with the Earth or Moon and the amount which remain gravitationally bound to the two. Additionally, the ability of this material to alter the Earth's night sky is examined. Particles are projected onto the night sky for Earth based observers. When combined with estimations for the flux due to reflected sunlight, the dust distribution is used to predict local sky brightness. The methods used to run the simulations, as well as the analysis required for particle density estimations and flux calculations and projections are described in Chapter 2. The results of the simulations and the subsequent analysis are shown in Chapter 3. Discussion of all the results, including additional simulations with radiation forces, as well as potential future work are presented in Chapter 4, while conclusions are provided in Chapter 5.

[6]These are likely interplanetary dust getting trapped, rather than material from the Moon.

Chapter 2

Methods

The dynamical behaviour of material in the cis-lunar environment is explored by running computational N-body simulations of particles ejected from the lunar surface. In total, 10,000 particles are released at random locations around the Moon with a velocity distribution that allows the particles to just escape the influence of the lunar gravity. The short and long-term results of the simulations are analyzed to understand where this material is transported, including if accumulation or over-densities are seen in any of the Lagrange point regions. The particles are also projected onto the sky for an observer on Earth to examine how the brightness of the night sky could be impacted by the reflection of sunlight by this material. It is important to point out that these simulated particles can be thought of as tracer particles. Each simulated particle may represent a large number of actual particles, all comparable in size and released with similar trajectories. The exact number depends on the mass that is assumed to be released. The analysis and results presented in this study are only for the simulated particles, but a number of the results can be scaled accordingly, as will be discussed in Chapter 4.

2.1 Dynamical Simulations

Simulations in this study are performed using REBOUND, a N-body simulator package for python which has its main routines written in C [29]. The default integrator for REBOUND, IAS15, was used for these simulations. IAS15 is a high order, non-symplectic integrator with an adaptive time-step that allows for increased precision during close approaches while minimizing the overall run time [30]. REBOUNDx, a package designed to incorporate additional effects into REBOUND, is included for simulations where radiation forces are taken into account [41]. REBOUNDx models the radiation forces based on Burns et al. [5], using

$$\mathbf{a} \approx \beta \frac{GM_{\odot}}{r^2} \left[(1 - \hat{\mathbf{r}} \cdot \mathbf{v}/c) \hat{\mathbf{r}} - \mathbf{v}/c \right]. \tag{2.1}$$

Here, $\mathbf{a}$ is the acceleration of the particle, $\mathbf{r}$ is the particle's heliocentric position vector, $\mathbf{v}$ is the heliocentric velocity, and c is the speed of light. The parameter β is the ratio of the solar radiation pressure force to the gravitational force experienced by a particle in orbit, given by

$$\beta \equiv F_r/F_g = 5.7 \times 10^{-5} Q_{pr}/\rho s, \tag{2.2}$$

where s and ρ are the particle radius and density in cgs units, respectively, and Q_{pr} is the radiation coefficient. The parameter β is thus large for very small particles and becomes negligible as the particle size increases. The primary results presented in Chapter 3 are for simulations of large particles where beta is assumed to be zero. However, separate simulations were run with a high beta (0.1), representing particles that are approximately a few to ten microns in diameter. These simulations were completed after a majority of this thesis was written, and thus the results are included in Section 4.2.

Individual simulations containing only one massless particle, along with the Sun, Earth, and Moon, are run in parallel for a total of 10,000 simulations. As the particles are massless, there are no interactions between the particles during the simulations. Therefore, provided the simulations have identical starting times, they can be run separately and subsequently combined for analysis to keep the computational times manageable. This parallelization is accomplished using the multiprocessing package in python. All simulations are performed on a 2020 MacBook Pro with an Apple M1 chip and 8 GB of ram, using 6 of the 8 cores available. The starting time for each simulation is set to be August 22, 2007, 01:14:00 TDB (2454334.551388889 JD), with the initial conditions for the Sun, Earth, and

Moon in the heliocentric ecliptic coordinate system obtained using NASA's JPL HORIZONS Web-Interface.[7] While initial conditions are defined in the heliocentric frame, the simulations are run in the center of mass frame, with REBOUND containing built-in functions to handle these transformations. Simulations are run for varying lengths of time with different archiving time-steps to allow for analysis of both the long-term behavior and higher temporally resolved short-term behavior. Particle collisions with the Sun, Earth, and Moon are tracked and recorded during the simulations within REBOUND using its built-in "line" collision search, which checks if the trajectory of two objects overlap during the time-step, assuming they are traveling straight. If a particle collides with one of the three large bodies, the particle is removed from the simulation. Particle on particle collisions are ignored for this study.

Rather than attempting to model specific mechanisms or processes that could eject material from the lunar surface, a simplified approach is taken. Particles are released in a random uniform spatial distribution spread evenly across the Moon, at an altitude of 100 km, using a method based on Shao and Badler [33]. This is done by first using python's random module to generate two random variables:

$$\begin{aligned} a &= \text{Uniform}[0,1], \\ b &= \text{Uniform}[0,1]. \end{aligned} \tag{2.3}$$

These random numbers, a and b, are then converted into angles:

$$\begin{aligned} \theta &= \arccos(2b-1), \\ \phi &= 2\pi a, \end{aligned} \tag{2.4}$$

where θ can range $[0,\pi]$ radians measured from the pole and ϕ is the azimuthal angle, ranging $[0,2\pi]$ radians. This sampling results in a uniform distribution across the Moon, assuming it is a perfect sphere. The particles are chosen to be initially 100 km above the lunar surface to ensure there are no strange interactions or overlaps between the Moon and the particles when the simulations begin.

[7] Orbital data retrieved from https://ssd.jpl.nasa.gov/?horizons on November 1, 2021. The arbitrary starting time was chosen for preliminary work that is not included here and is kept purely for convenience.

A velocity distribution is assigned to the particles, v_{kick}, relative to the Moon's orbital velocity about the Sun, with a magnitude calculated as follows:

$$v_{kick} = \sqrt{{v_{min}}^2 + {v_{random}}^2}, \tag{2.5}$$

where v_{min} is the escape velocity of the Moon from an altitude of 100 km and v_{random} is a random velocity drawn from a Rayleigh distribution with a mode of 1 m/s. The Rayleigh distribution is chosen for convenience and to generate a dispersion among the velocity magnitudes, while the choice of 1 m/s is to give the particles a speed just above the escape speed, on average. The particles' initial velocity vector is not directly perpendicular to the lunar surface, but rather, a random direction within a cone is used. The launch angle is tilted in a uniform random direction with a uniform random angle from zenith between $[0, \frac{\pi}{4}]$ radians, with 0 corresponding to a perpendicular ejection.

2.2 Coordinate Transformations

One of the first steps for analyzing the simulation results is transforming the particles, along with the 3 larger bodies, into different frames of reference. Examples include the geocentric and selenocentric frames, which allow for observing the trajectory and behavior of the particles relative to the Earth and lunar orbital planes. Different combinations of rotations, combined with translations, can allow the simulations to be viewed from a variety of different frames of reference. Two rotation matrices are required to accomplish the transformations in this study:

$$\begin{aligned} R_x(\Theta) &= \begin{bmatrix} 1 & 0 & 0 \\ 0 & \cos\Theta & -\sin\Theta \\ 0 & \sin\Theta & \cos\Theta \end{bmatrix}, \\ R_z(\Phi) &= \begin{bmatrix} \cos\Phi & -\sin\Phi & 0 \\ \sin\Phi & \cos\Phi & 0 \\ 0 & 0 & 1 \end{bmatrix}. \end{aligned} \tag{2.6}$$

Here, $R_x(\Theta)$ and $R_z(\Phi)$ represent rotation matrices for rotations about the x-axis and z-axis, respectively, for the given angles, Θ and Φ.

2.2.1 Lunar Rotating Frame

A majority of the analysis is performed in the Moon's rotating frame about the Earth, where the xy-plane is aligned with the lunar orbital plane, such that the Earth and Moon are along the x-axis and the Earth-Moon barycenter is at the origin. To transform the simulations into the Moon's rotating frame, they are first transformed into the Earth's rotating frame about the Sun. Beginning in the heliocentric frame, the simulations are rotated about the z-axis by the longitude of Earth's ascending node, effectively aligning the Earth's orbital nodes along the x-axis. Next a rotation is performed about the x-axis equal to the Earth's inclination, placing the Earth's orbital plane in the xy-coordinate plane. The Earth can then be rotated to the x-axis by applying another z-axis rotation, this time with an angle equal to the Earth's true anomaly plus the Earth's argument of pericenter. Finally, a translation in the negative x-direction, equal to the Earth's instantaneous heliocentric distance, results in an Earth-centered rotational reference frame, with the Sun always on the negative x-axis.

Applying similar rotations to this new Earth-centered, or geocentric, frame, but with respect to the Moon, will result in the simulations being transformed into the Moon's rotational frame. The lunar orbital elements used here are calculated in the geocentric frame. Beginning from the geocentric frame, a z-axis rotation is applied, equal to the longitude of the Moon's ascending node. With the Moon's nodes now along the x-axis, the simulations can be rotated about the x-axis by the Moon's inclination to place the lunar orbital plane in the xy-plane. A final z-axis rotation equal to the Moon's true anomaly plus the Moon's argument of pericenter places the simulations into the Moon's rotating frame, with the Earth at the origin and the Moon along the x-axis in the xy-plane. The lunar rotating frame's origin is then translated to the Earth-Moon's barycenter, as is common convention.

2.2.2 Sky Projection

A different series of translations and rotations are performed to place an Earth based observer at the origin of a new frame, which allows for easier computation of the positions of the Sun, Moon, and particles across the sky. For this study, the observer is assumed to be located near Vancouver, British Columbia (49° N, 123° W). Beginning in the simulation's heliocentric frame, the coordinates are translated to have the origin centered on the Earth. A rotation about the x-axis of this translated frame, by the Earth's obliquity relative to the ecliptic plane, places the Earth's north pole along the z-axis. This can be done as the simulations are originally in the ecliptic coordinate system. At this point, a rotation about the z-axis based on the time of the simulation and the given observer's longitude is performed to place the observer along the y-axis. A final x-axis rotation based on the observer's latitude is then used to put the observer on the x-axis as well. Subtracting the z-values by the Earth's approximate radius (6471 km) places the observer at the origin. In this frame, the observer's zenith is along the z-axis, north is in the positive y-direction, and east is in the positive x-direction.

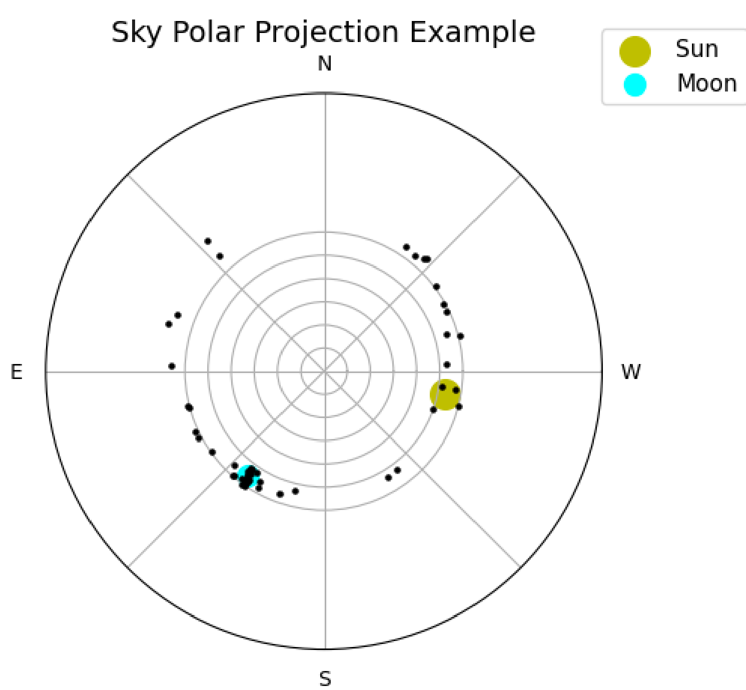

Figure 2.1: An example of a polar projection of the Sun, Moon, and particles from an observer's perspective on Earth. The inner grey rings represent steps of 15° from the zenith, with the last inner ring representing the visible horizon. In this example, the Sun is just beginning to set along the western horizon, while the Moon is rising out of the south-east.

A polar projection is used to visualize the position, and ultimately brightness, of the particles from the observer's perspective, with an example shown in Figure 2.1. This projection represents what an observer who is lying on their back with their head pointed north would see. To accomplish this, the signs of the x-coordinates are flipped to have west pointed in the positive x-direction. The radius of the polar projection plot is the angle of the object relative to the observer's zenith, with objects at a radius greater than 90° being considered below the horizon. The horizon is indicated by the final grey inner ring in the example above, with each ring representing a step of 15°. The outer black ring marks 180°, which is actually just a point directly below the observer, representing anti-zenith. These projections were tested by verifying the position of the Sun and the Moon at different times.

2.3 Time Series Analysis

When running the simulations, snapshots are archived at constant time intervals for analysis. Simulations that are run for 30 days are archived four times per simulated day, while yearlong simulations have snapshots saved just once a day. The spatial distribution of the particles is plotted and analyzed from a variety of reference frames at different times during the simulations. Special attention is paid to analyzing particle densities around the Earth-Moon Lagrange points and the corresponding density evolution. The brightness of these particles is of interest as well, so their projections onto the sky of an Earth based observer are also analyzed at different times. In the following subsections, the methods for obtaining particle volume densities, determining Lagrange points, and estimating sky brightness are all discussed.

2.3.1 Kernel Density Estimator

A cubic spline kernel density estimator, based on Monaghan [26], is used to determine the spatial densities of particles at any given location. Here, the density at a given point j is approximated by

$$\rho_j = \sum_{i}^{N} \frac{1}{\pi h^3} \begin{cases} 1 - \frac{3}{2}(\frac{r_{ij}}{h})^2 + \frac{3}{4}(\frac{r_{ij}}{h})^3 & \text{if } 0 \leq \frac{r_{ij}}{h} \leq 1; \\ \frac{1}{4}(2 - \frac{r_{ij}}{h})^3 & \text{if } 1 \leq \frac{r_{ij}}{h} \leq 2; \\ 0 & \text{otherwise,} \end{cases} \tag{2.7}$$

where N is the number of interpolants, r_{ij} is the distance to particle i from the point j, and h is the length scale. The length scale is defined as half the radius of a sphere that is centered at point j and contains the closest 32 particles. A kd-tree is used to query the 32 closest particles, using an algorithm in SciPy's spatial algorithms and data structures package, described by Maneewongvatana and Mount [24].

To avoid the kernel from including too distant of particles, a maximum distance limit is placed on the length scale, which is 30,000 km for this study. Due to the nature of kernel, this has the effect of excluding any particle that is greater than 60,000 km away from the point of interest. This value is chosen as it is the approximate distance of L1 and L2 from the Moon.

2.3.2 Lagrange Points

The three collinear Earth-Moon Lagrange points (L1, L2, and L3) are calculated assuming the circular restricted three body problem holds. This is not strictly correct due to the Moon's eccentricity of about 0.05 but is sufficient for the calculations here. Within the Moon's rotating frame, the origin is assumed to be the Earth-Moon center of mass with the Earth at $x = -\mu$ and the Moon at $x = 1 - \mu$ in units of lunar distances, where $\mu = \frac{m_2}{m_1+m_2}$, with m_2 the smaller of the two masses, which is the Moon in this case. Numerically solving the equation of motion

$$0 = x - \frac{(1-\mu)(x+\mu)}{|x+\mu|^3} - \frac{\mu(x-1+\mu)}{|x-1+\mu|^3}, \tag{2.8}$$

results in the three real roots corresponding to the x-positions of the three collinear Lagrange points.

The L4 and L5 Lagrange points are approximated to be $\pm 60^\circ$ in front of and behind the Moon, assuming again an instantaneous circular orbit. These two points can also be determined analytically from the CR3BP setup, but the approximation used here is sufficient for the depth of this study.

As noted, the CR3BP is assumed for these calculations, which is not exact due to the Moon's eccentricity. To accommodate this variation, including the change in the Earth-Moon distance with time, the positions of the Lagrange points are uniquely calculated for each time-step analyzed. As a result, the Lagrange points oscillate radially, with respect to the Earth in the Moon's rotating frame, at the same rate as the Moon.

2.3.3 Sky Brightness Estimates

The flux of sunlight that reaches the Earth after reflecting off a particle is approximated as

$$f_p = S_I P(\omega) A_p SA_p / (\pi {d_{Earth}}^2). \tag{2.9}$$

Here, S_I is the solar irradiance value, set to be 1373 W/m^2 for this study, representing the total amount of solar energy per square meter reaching Earth every second, given here for the full solar spectrum. This is kept constant for all the particles in these simulations, as they are all approximately 1 au from the Sun. The phase function of the particles, $P(\omega)$, represents how much light is reflected relative to the angle of the Sun, particle, and observer. Additionally, A_p is the Bond albedo of a particle 'p', SA_p is the particle's cross-sectional surface area, and d_{Earth} is the distance from the particle to Earth. For this study, several key assumptions are required. A linear phase function is assumed, such that $P(\omega) = 1$ for particles 180° away from the Sun relative to the observer, while $P(\omega) = 0$ for particles with a phase angle of zero. Particles are assumed to have an albedo similar to the Moon ($A_p = 0.14$) [25] and a radius of one millimeter for these flux calculations. The cross-sectional surface area is calculated assuming the particles are spheres.

Chapter 3

Results

The short and long-term behavior of the simulated particles, including density estimates at the Lagrange points and collision statistics, are presented in Section 3.1. Polar projections of the particles onto the night sky for an Earth based observer are shown in Section 3.2, including 2d binned projections of the expected solar flux scattered off the particles. Comparisons of simulations with and without radiation forces (β = 0.1 vs β = 0.0) are discussed in Section 4.2. However, the value of β = 0.1 is an extreme case and should be taken as an approximate upper limit. The case of β = 0.0 will apply to a wide range of particle sizes and has the greater potential to be threatening to cis-lunar operations. As will be shown in Section 4.2, such particles will also remain in the cis-lunar environment longer than very high beta particles, and thus, could contribute more to sky brightness in the long term. For these reasons, all results presented in this chapter are for simulations with no radiation forces on the particles ($\beta = 0.0$).

3.1 Dynamical Behavior of Particles

Figure 3.1 shows the release and subsequent spread of 10,000 particles in the xy-plane of the Moon's rotating frame at six different times during the first 10 days of the simulations[8]. The origin has been translated to be centered on the Moon to examine the initial trajectory of the particles relative to the Moon. The Earth

[8] The number of particles shown decreases over time due to collisions.

XY Particle Distribution in the Moon's Rotating Frame over 10 Days

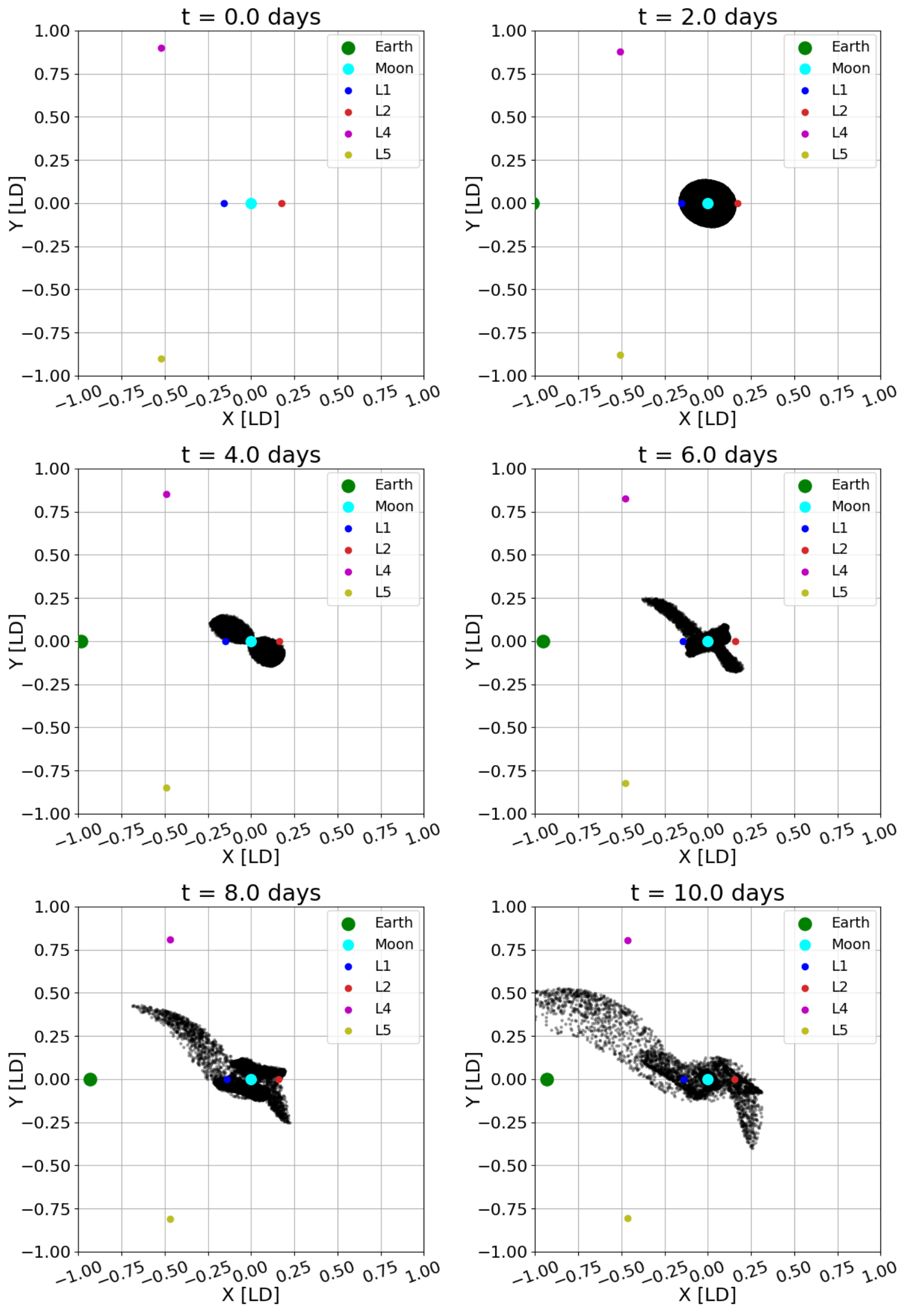

Figure 3.1: The xy-positions of the debris particles, Earth, Moon, and four of the five Earth-Moon Lagrange points, in the Moon's rotating frame, with the origin centered on the Moon, over the course of 10 days.

and the four nearby Lagrange points have been included for reference. The axes are labeled in units of lunar distance [1 LD $\approx$ 3.844e5 km $\approx$ 0.0025 au], which is defined as the average distance between the Earth and the Moon.

During the first few days after release, the particles can be seen expanding isotropically away from the Moon, reaching just beyond the L1 and L2 Lagrange points before the particles begin to shear. Two trails of particles continue away from the Moon in opposite directions, through the vicinity of L1 and L2. Some particles in these trails escape the lunar gravity well and becoming increasingly influenced by the gravity of the Earth and the Sun. Not all particles escape, with some falling back and colliding with the Moon after several days in the lunar orbital environment, while others enter lunar orbits.

Ten days after release, some particles have traveled beyond a lunar distance, stretching past the Earth, while over 40% have already crashed back into the surface of the Moon. The earliest, as well as the majority, of the impacts occur on days four and five, with almost 3600 lunar collisions recorded on just these two days. Although no particles travel very close to L4 or L5 during the first 10 days, the same cannot be said about the two nearby collinear Lagrange points. L1 and L2 both see a steady stream of particles flowing directly through them during the first 10 days. This can be further seen through the particle density evolution at the Lagrange points.

Figure 3.2 shoes the kernel density estimations for L1 and L2 during the first 10 days of the simulations. The densities for both points first peak about two days into the simulations, which corresponds to when the particles are first expanding through the two points, as seen in Figure 3.1. Between days four and six there is a decrease seen in the density estimations, which is supported by the xy-positions of the particles at this time. The following days show an increase in particle densities at L1 and L2, although never exceeding the initial peak values from around day two. While the densities at L1 and L2 differ at times, they follow a similar pattern and reach comparable peak values. The remaining three Lagrange points do not produce any density estimates during this time as they do not have any particles close enough to be included within the maximum smoothing length.

The distribution of the particles during the first 30 days of the simulations is shown in the xy-plane in Figure 3.3, as well as in the xz-plane in Figure 3.4. For

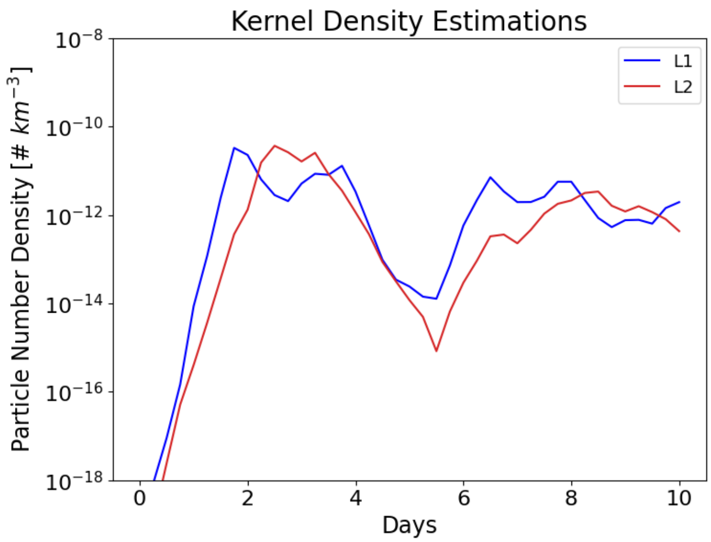

Figure 3.2: The kernel density estimations for the L1 and L2 Earth-Moon Lagrange points during the first 10 days of the simulations. The density is given in number of simulated particles per cubic km.

both figures, the origin is centered on the Earth-Moon center of mass. The xy-view shows the two previously seen trails further extending, creating two different populations. The trail that originally extended through L1 is now in orbit around the Earth, staying within L3, L4, and L5, and wrapping completely around back to L1 within about three weeks. The other trail of particles continues to drift further away from the Earth-Moon system, appearing to orbit the pair from outside the Lagrange points. All the particles seem to stay close to the lunar orbital plane during the first few weeks of the simulations, but by the end of the first month, the outer most particles extend to almost half a lunar distance in both directions.

The kernel estimations of the particle densities at the Lagrange points over 30 days is shown in Figure 3.5. During the first month of the simulations, the L3, L4, and L5 Lagrange points appear to stay clear of particles, while the L1 and L2 points seem to exhibit a slowly decreasing amount of material. Large variations exist within the overall trend, including an order of magnitude spike in the L1 density around day 14, which is due to a dense cloud of particles in lunar orbit passing through L1. The remaining three Lagrange points are not included for this

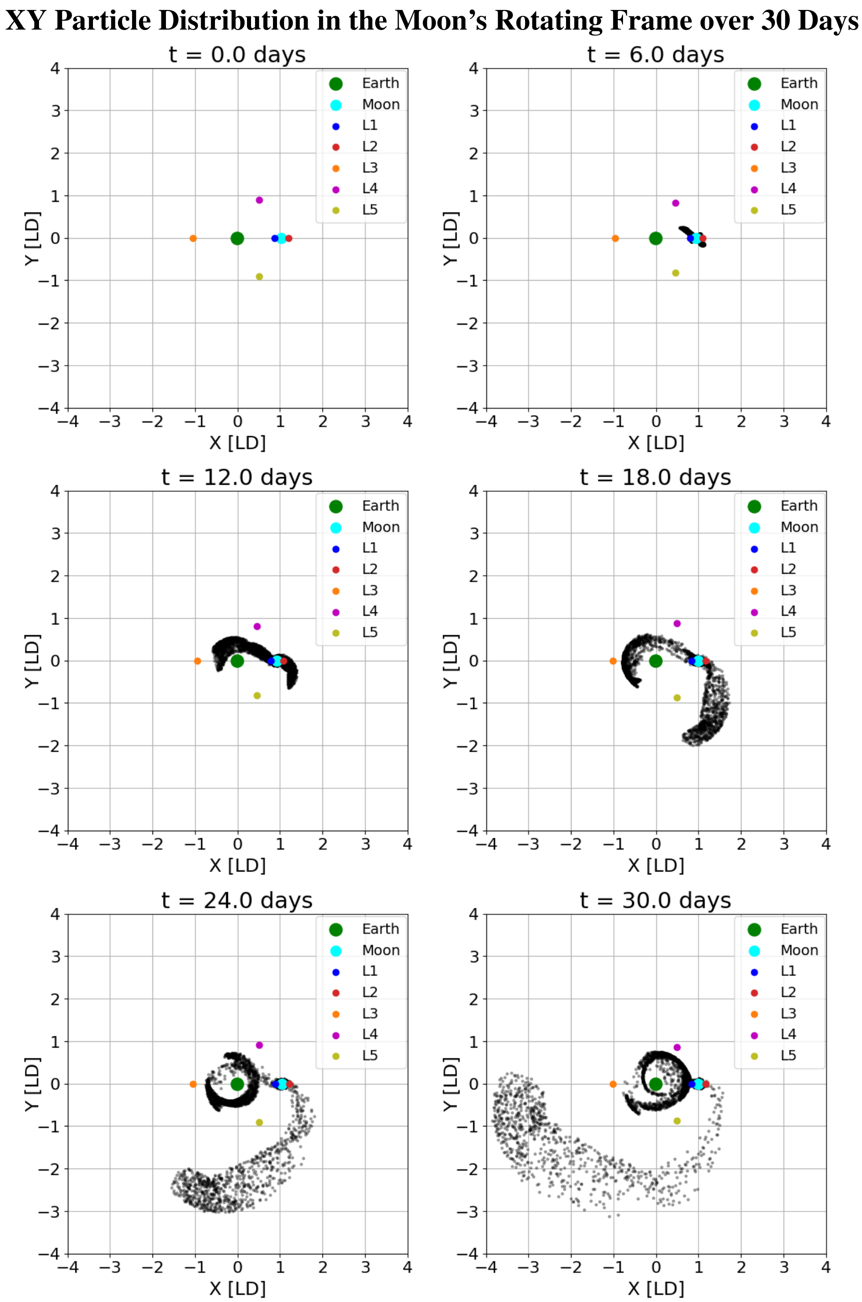

Figure 3.3: The xy-positions of the debris particles, Earth, Moon, and the five Earth-Moon Lagrange points, in the Moon's rotating frame, with the origin at the Earth-Moon center of mass, over the course of 30 days.

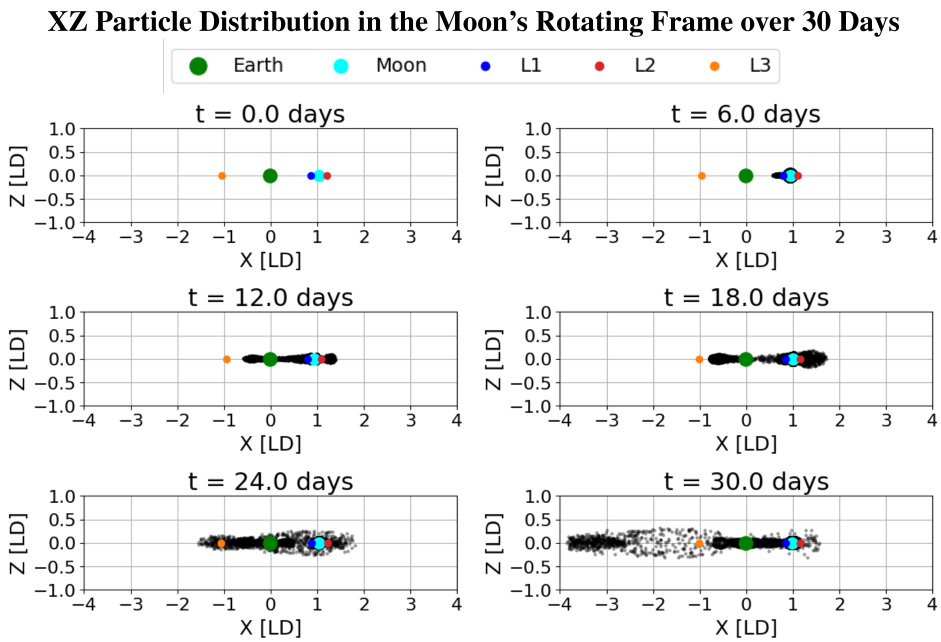

Figure 3.4: The xz-positions of the debris particles, Earth, Moon, and the three collinear Earth-Moon Lagrange points, in the Moon's rotating frame, with the origin at the Earth-Moon center of mass, over 30 days.

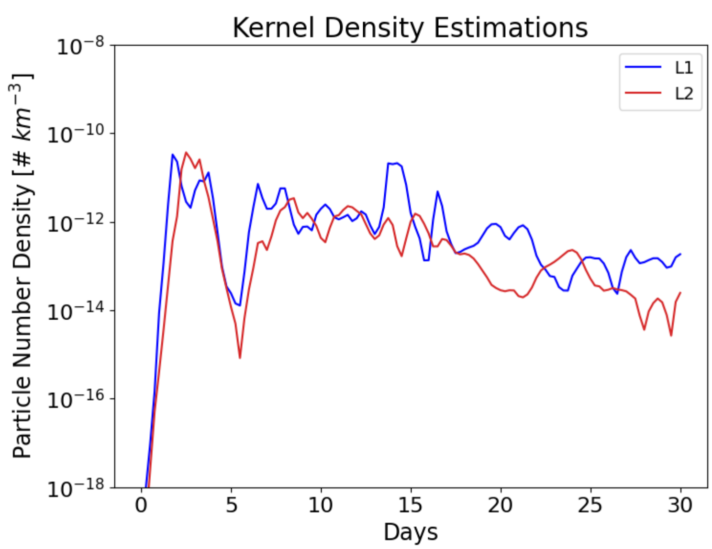

Figure 3.5: The kernel density estimations for the L1 and L2 Earth-Moon Lagrange points during the first 30 days of the simulations.

plot once again as there are still no particles within the maximum scale length of the kernel for each point during this time. After 30 days, almost half the particles (48.9%) have collided with the Moon, while none is found to have yet collided with the Earth (or Sun).

As noted in Section 2.3, the simulations are further propagated up to one year, however, the output is less frequent. This nonetheless allows one to get a better understanding of the longer-term behavior of the particles. Figure 3.6 shows the xy-

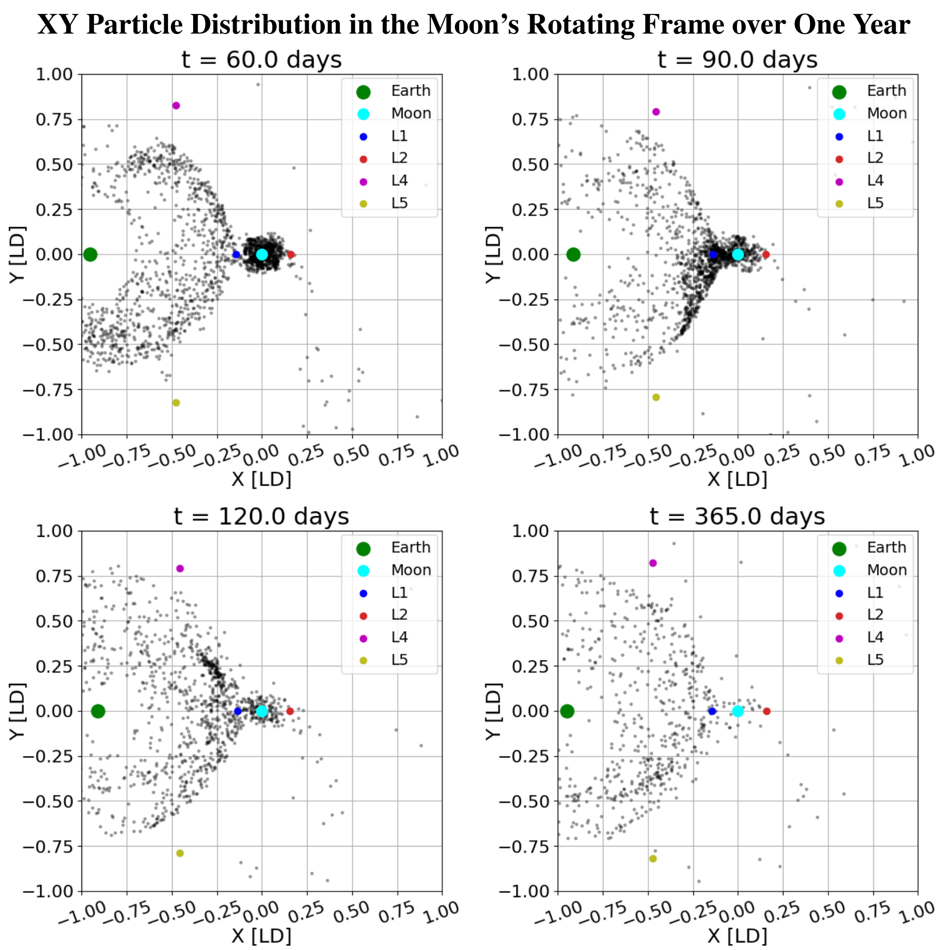

Figure 3.6: The xy-positions of the debris particles, Earth, Moon, and the four nearby Earth-Moon Lagrange points, in the Moon's rotating frame, with the origin centered on the Moon, over the course of a year.

positions of the particles relative to the center of the Moon, while Figure 3.7 shows the xy-positions of the particles at the same times, but with respect to the Earth-Moon center of mass. In the Moon centered frame, particles are found to remain in lunar orbits for the full year, although there are considerably fewer particles after a year than at 60 days. After 60 days, there are about 800 particles within the Moon's hill sphere, while after a year there are only 26. Figures 3.6 and 3.7 both show that

XY Particle Distribution in the Moon's Rotating Frame over One Year

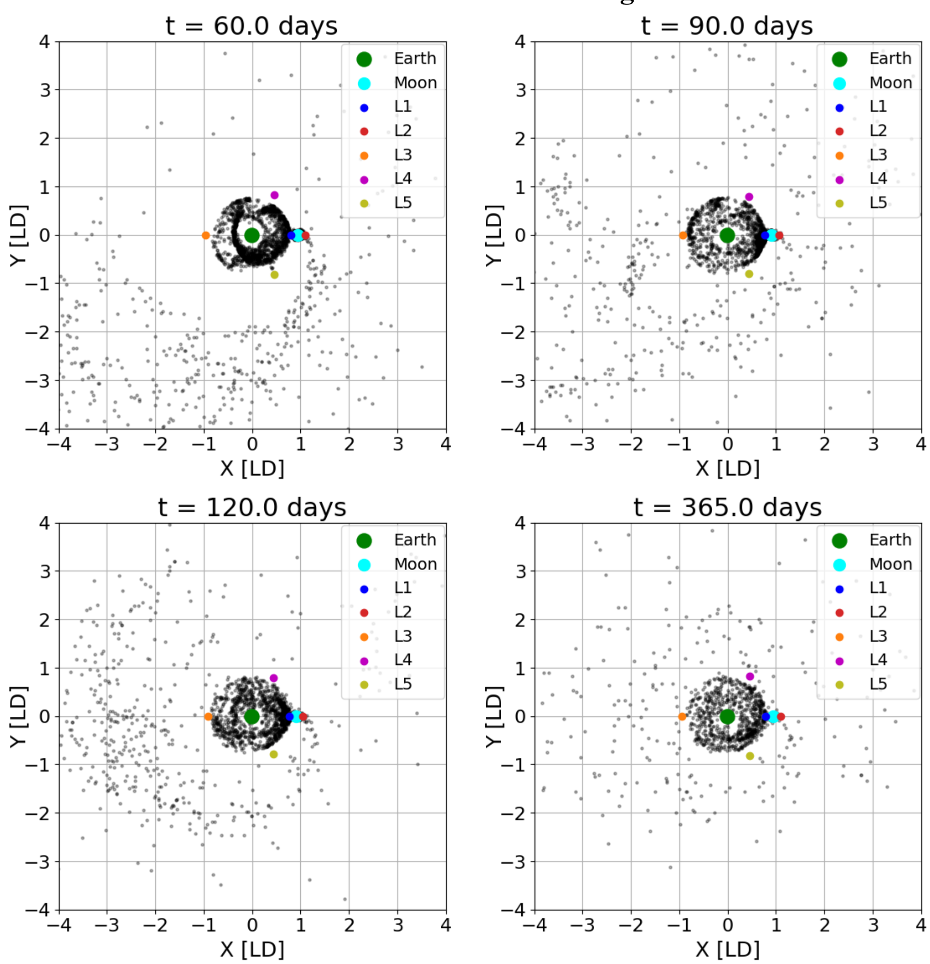

Figure 3.7: The xy-positions of the debris particles, Earth, Moon, and the five Earth-Moon Lagrange points, in the Moon's rotating frame, with the origin at the Earth-Moon center of mass, over the course of a year.

large numbers of particles remain in orbit around the Earth during the full first year, with less of a decrease seen in comparison to particles in lunar orbit. Particles are not bound to either orbit, as several are often seen transferring between different orbits about the Earth and the Moon.

While the majority of the particles orbiting the Earth appear to be within the Lagrange points, there remains a scattered population of particles extending beyond the Lagrange points after one year. Once again, the kernel can be used to estimate the particle densities found at the five Earth-Moon Lagrange points to determine if particles are crossing through any of the points. Figure 3.8 shows the density estimations for the five Lagrange points during one year of the simulations. After about 200 days, the particle density around L1 and L2 becomes roughly constant on average, but with order of magnitude variations over weekly timescales. L1 retains a slightly higher density compared with L2, more noticeably during the second half of the year. After about two months, the other three Lagrange points

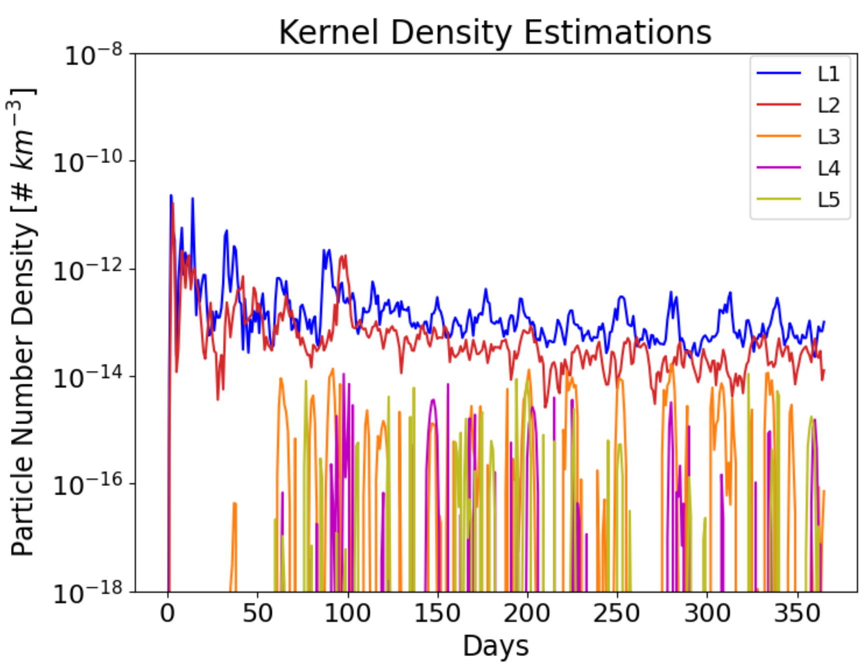

Figure 3.8: The kernel density estimations for all five of the Earth-Moon Lagrange points during one year of the simulations.

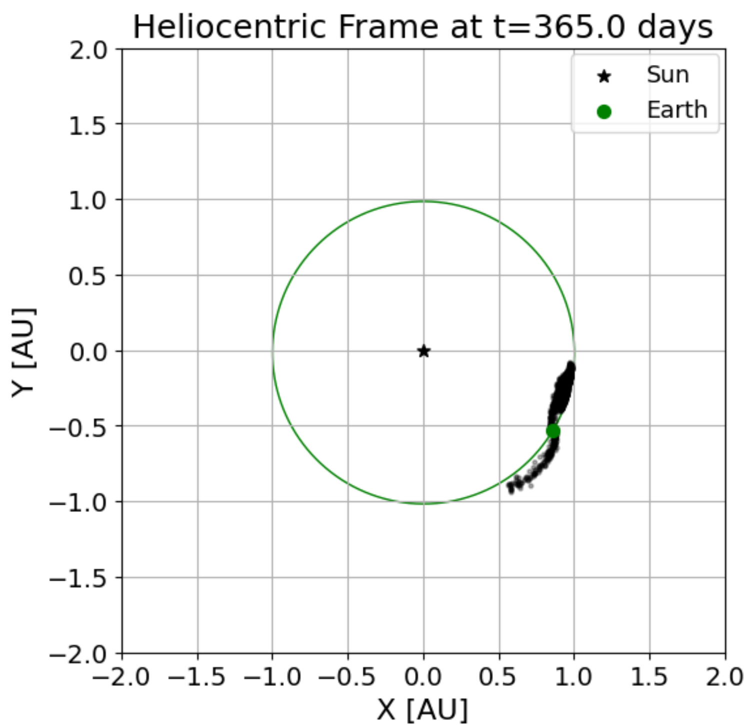

Figure 3.9: The xy-positions of the debris particles, the Earth, and the Sun, in the simulation's original heliocentric frame, one year after the particles were released. The Earth's orbit is shown with the green line to give reference for the radial spread of the particles.

begin to sporadically encounter particles, at times reaching levels that are comparable to the L1 and L2 densities.

By the end of the year, only 25% of the initial particles remain, with a large number of those appearing to escape onto heliocentric orbits, shown in Figure 3.9. Most of the particles that remain gravitationally bound to the Earth-Moon system during the simulations eventually get swept up by the two bodies. In total, 21 particles collide into the Earth, while 7479 collided with the Moon. Only about 1000, or 40%, of the remaining particles are within the Earth-Moon hill sphere after one year. The particles that do escape are slowly shearing out in both directions and will eventually spread throughout the Earth's entire orbit in approximately 5-10 more years.

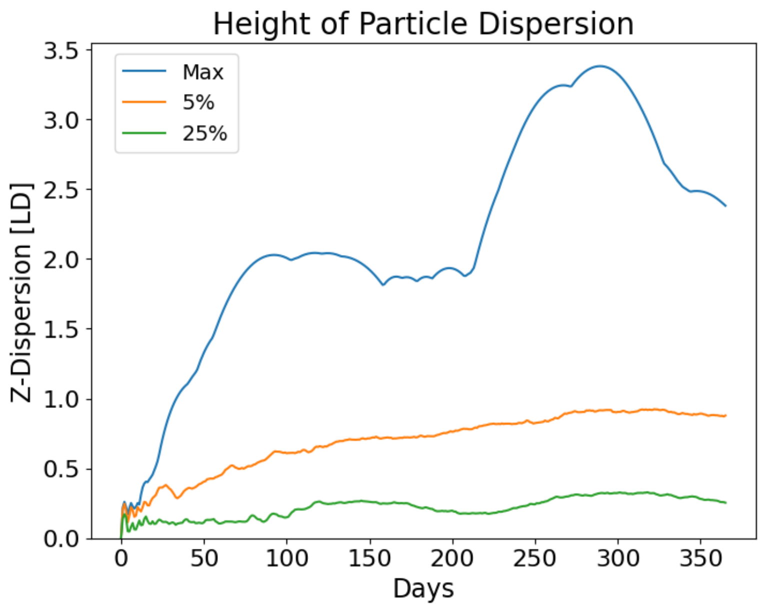

Figure 3.10: The maximum z-distance, normal to the Earth's orbital plane, between any two particles during one year of the simulations. The blue line represents the z-distance between the two furthest particles. The orange line is the z-distance between the two furthest particles if 5% of the particles at either extreme are excluded, while the green excludes 25% of the particles at either end.

Figure 3.10 shows the maximum z-distance between any two particles, normal to the Earth's orbital plane, during the simulated year. The blue line is the true maximum between any of the particles, while the orange and the green lines seek to exclude any outliers, as well as demonstrate the spread of the bulk of the material. The orange line excludes the furthest 5% of the particles at either end, while the green excludes 25% of both ends. The largest z-distance between two particles during the first year was almost 3.5 lunar distances. This is likely due to a stray particle kicked out of the ecliptic plane after a close encounter with the Earth or the Moon. The orange lines shows that the majority ($\geq 90\%$) of the particles are dispersed less than one lunar distance, normal to the ecliptic, for the entire year.

3.2 Night Sky Projections

At various points throughout the simulations, the particles are projected onto polar maps of the sky to determine if and where on the sky the particles would be visible at night for an Earth based observer. Particles are generally visible (above the horizon) for most nights, apart from a few of the first nights of the simulations during the new moon phase, when the particles are not yet spread beyond the lunar hill sphere. After the streams of particles become sheared out during the first few months, any given night will have roughly half the particles visible above the horizon, usually oscillating between 30% and 70%.

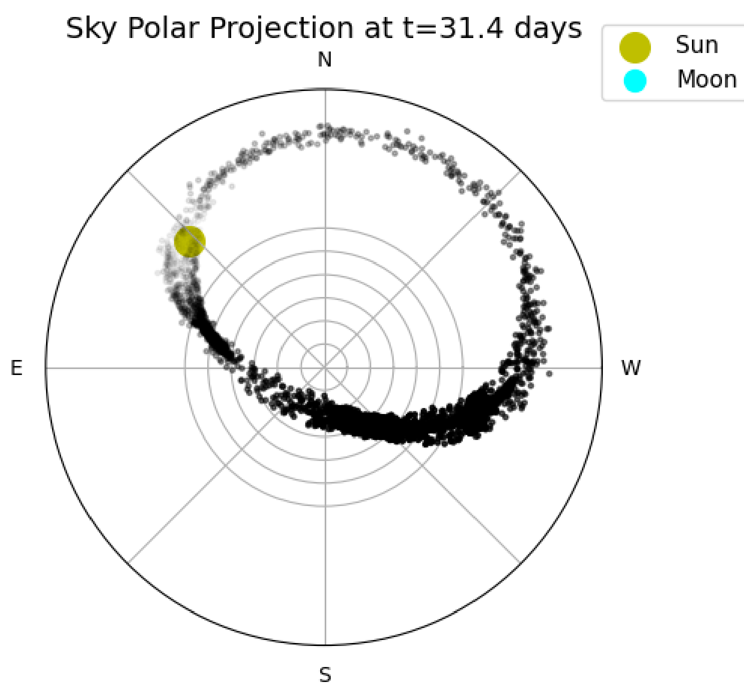

Figure 3.11: The polar projection of the particles, the Sun, and the Moon, at night for a northern hemisphere observer, approximately one month into the simulations. The inner grey rings are at 15° steps from the zenith, with the outer grey ring representing the visible horizon. The Moon is covered in this plot by the particles just below the south-west horizon. Particles are shaded relative to their solar phase angle.

Occasionally, the particles create a large stream across the night sky, with an example of this shown in Figure 3.11. As a reminder, this and the subsequent plots in this section are for an observer near Vancouver, Canada (49° N, 123° W). Here, the particles are plotted with an alpha corresponding to their phase angle, such that particles that would appear close to the Sun in the sky are more transparent and light grey in color. Particles that are on the opposite side of the Earth from the Sun, and thus would reflect a large amount of light towards the observer, are shaded the darkest. The local time of this projection for the observer near Vancouver is approximately 4:00 am in September, so the Sun, which will rise above the eastern horizon in a couple hours, is where it is expected to be. The Moon is hidden behind the particles in this plot, just below the horizon in the south-west.

Figure 3.12 shows a polar projection of the bolometric flux of reflected sunlight

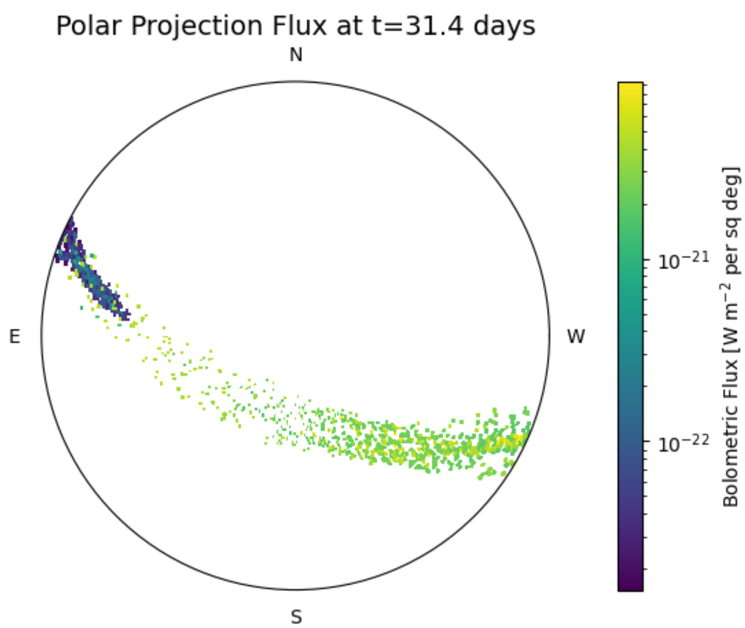

Figure 3.12: The flux of reflected sunlight from particles visible above the horizon approximately one month into the simulations. The plot is divided into bins 1° by 1° in size, with the color mapping normalized on a log scale. The Sun and the Moon are both below the horizon. Note this is the bolometric flux.

that would reach the Earth from these particles, calculated using Equation 2.9, and filtered to just show the visible sky above the horizon of the observer. The plot has been divided into a 2d grid, with each bin one square degree in size. As the flux values are calculated in units of W/m^2, the units of each bin in the figure are therefore W/m^2 per square degree. The solar irradiance value listed in Section 2.3.3 accounts for the full solar spectrum and not just visible light. Therefore, these are bolometric flux values, which can ultimately be scaled to visible flux values, as discussed further in Section 4.3. The color mapping of the bins is normalized on a log scale, with the minimum and maximum non-zero bin values set as the limits. At this time in the simulation, the Sun and the Moon are both below the horizon, so the sky would be dark, and nothing would be concealing the particles.

A wide range of values are seen in the previous figure, driven largely by the varying distances to the particles from the Earth, with the minimum and maximum flux separated by almost three orders of magnitude. Further particles will have a greater distance for the reflected light to disperse and therefore will be less bright. Different phase angles will also add to this variation, although not to the same extent. The differing phase angles accounts for the gradient of yellow and green seen across Figure 3.11, while the darker blue patch extending from the eastern horizon is a different population of particles further away.

While particles are found to be visible in the sky almost every night of the simulation, they do not always appear as a streak across the sky, and at times they appear to wrap around the horizon, as seen in Figure 3.13. Here, an even greater difference in flux values is seen, with values both higher and lower than the previous plot. This is likely due to the particles having more time to disperse, and therefore the particles are both closer and further to the Earth than earlier in the simulations. The dark blue streak seen above the south-west horizon is some of the particles that are seen escaping into heliocentric orbit in Figure 3.9, with closer particles orbiting the Earth passing in between. The Sun and the Moon are again below the horizon for this plot.

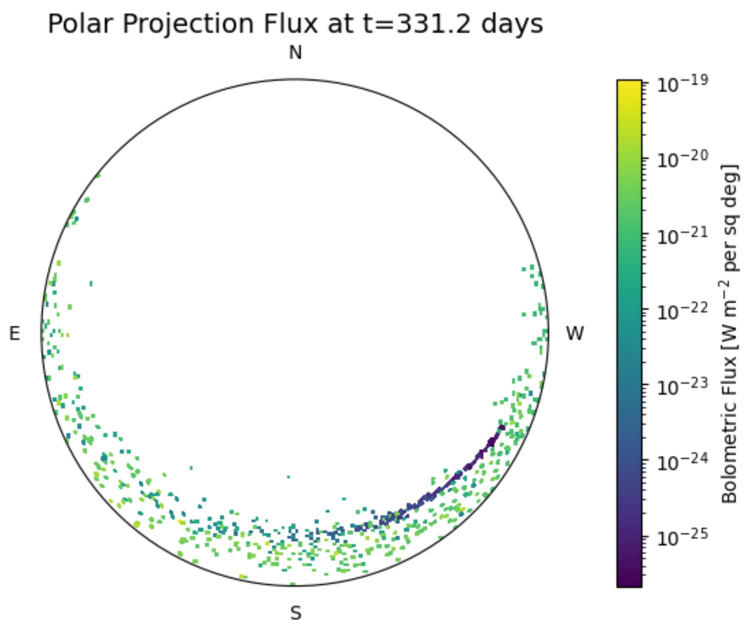

Figure 3.13: The bolometric flux of reflected sunlight from particles visible above the horizon, almost one year into the simulations. The plot is divided into bins 1° by 1° in size, with the color mapping normalized on a log scale. The Sun and the Moon are both below the horizon.

Chapter 4

Discussion

4.1 Particle Behavior

The simulations presented in Chapter 3 for particles with no radiation forces included ($\beta = 0.0$) showed that three quarters of the initial particles eventually collided with the Moon or the Earth. A large number of particles fall back towards the Moon during the first week, with days four and five recording almost half of the total collisions that occur in the first year. The collisions will likely occur at different locations on the Moon than where the particles are released from, impacting at speeds comparable to their ejection velocities. Only 0.2% of the total particles released are found to collide with the Earth during the first year.

Particles that avoid collisions can have a number of different pathways. The simulated particles are observed to expand away from the Moon in all directions for about two days before they begin to spread. Two streams of particles extend away from the Moon in opposite directions during the first several weeks due to shear, while another population of particles appears to remain in orbit about the Moon. One stream enters into orbit around the Earth inside of the Earth-Moon Lagrange points, with some particles occasionally transferring back and forth into lunar orbits. The other stream wraps into a larger Earth orbit, remaining outside the Lagrange points, and eventually scattering into the greater cis-lunar environment and beyond. About 15% of the initially released particles are able escape the Earth's hill sphere, entering into heliocentric orbits similar to the Earth's. After one year, roughly 1000 of the initial 10,000 particles remain in orbit about the Earth, while only a few dozen still orbit the Moon. Most particles remain within a lunar distance from the ecliptic in the z-direction, with the largest dispersion reaching just under 3.5 lunar distances.

Once the initial expansion of particles reaches the L1 and L2 Lagrange points after just a couple of days, a continuous presence of material is seen at the two points. Both reach their peak densities during this initial expansion at comparable levels before trending down. After several months, L1 appears to retain higher densities, likely a result of the larger population of particles in orbit about the Earth than the Moon. Particles eventually start to cross through L3, L4, and L5 after a couple of months, with scattered peaks seen for all three, some briefly reaching values similar to L1 and L2. No particles seem to remain in any of these three points, as all the density measurements are spikes, nor is residency of particles at those locations expected based on energetics, at least from the point of view of the CR3BP.

As mentioned briefly at the start of Chapter 2, the simulated particles discussed here can also be thought of as tracer particles representing a larger number of actual particles. With this assumption, the reported kernel density values could be scaled directly by the number of actual particles represented by one simulated particle. It is also important to note that the results here assume the particles are large enough to neglect the radiation forces acting on them. We will now see in the next section, smaller particles with non-negligible beta values can exhibit differing behavior.

4.2 Radiation Forces

Identical simulations are run with the sole difference being that the particles are now subjected to radiation forces throughout the simulations. The particles are given a large beta value ($\beta = 0.1$), corresponding to particles that are about 10 microns in diameter, assuming a density of 1.4 g/cc and $Q_{pr} \approx 1$. The Earth and the Moon are both still assumed to have no radiation forces acting on them ($\beta = 0.0$).

Figure 4.1 shows that the high beta ($\beta = 0.1$) particles which initially escape the lunar gravity do not behave like the escaping particles with no radiation forces ($\beta = 0.0$). The influence of the radiation forces is seen immediately, with the par-

XY Particle Distribution in the Moon's Rotating Frame at 10 Days

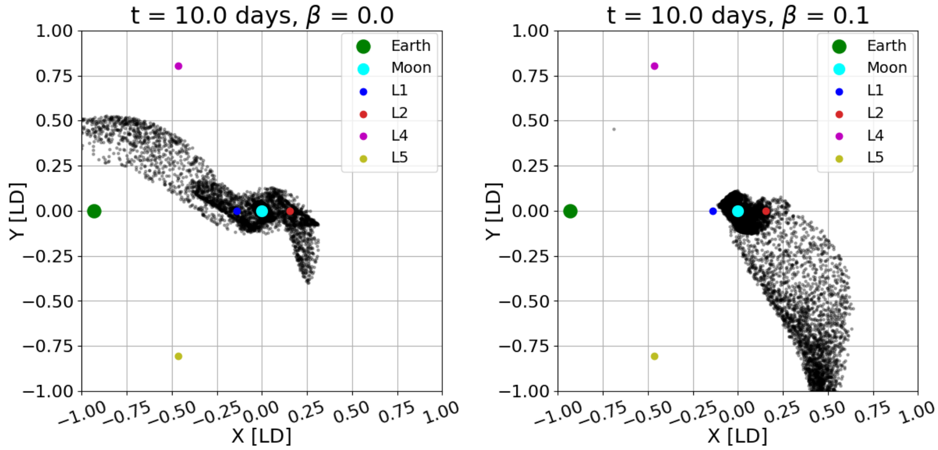

Figure 4.1: The xy-positions of the debris particles, Earth, Moon, and four of the five Earth-Moon Lagrange points in the Moon's rotating frame, with the origin centered on the Moon, at 10 days, for two different βs.

ticles stretching away from the Moon in one direction, rather than in two opposite directions as seen before. In fact, these particles are no longer bound to the Earth-Moon system and begin to expand away from the Sun. Due to the sudden exposure to radiation forces upon leaving the lunar surface, the particles' heliocentric semi-major axes are instantaneously increased. Thirty days into the simulations, the cis-lunar environment looks noticeably different. Figure 4.2 shows the Earth is unable to capture the same population of particles found to orbit within the Lagrange points in the original ($\beta = 0.0$) simulations.

The z-distribution of the particles in the lunar orbital plane is seen to increase for the particles exposed to the radiation forces, shown in Figure 4.3. This trend also appears for the dispersion of the particles, normal to the Earth's orbital plane, throughout the simulations as seen in Figure 4.4. Not only are the maximum z-distances of $\beta = 0.1$ particles much greater than the $\beta = 0.0$ particles, radiation forces disperse the bulk of the particles as well.

One year after the particles have been released, the simulation states are quite different. About 20% more of the initial particles subjected to radiation forces avoid collisions with the Earth and the Moon. Interestingly, almost 700 particles

XY Particle Distribution in the Moon's Rotating Frame at 30 Days

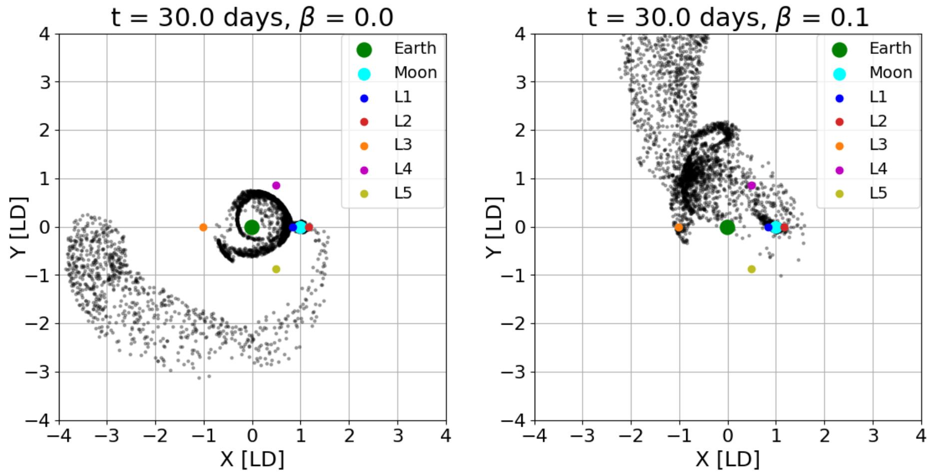

Figure 4.2: The xy-positions of the debris particles, Earth, Moon, and the five Earth-Moon Lagrange points in the Moon's rotating frame, with the origin at the Earth-Moon center of mass, at 30 days, for two different βs.

XZ Particle Distribution in the Moon's Rotating Frame at 30 Days

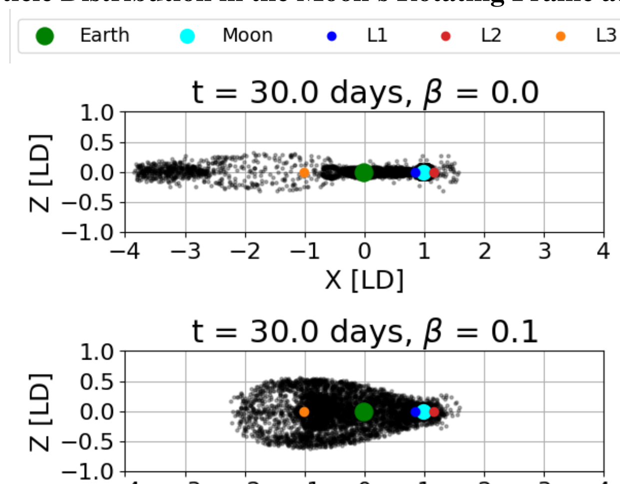

Figure 4.3: The xz-positions of the debris particles, Earth, Moon, and the five Earth-Moon Lagrange points in the Moon's rotating frame, with the origin at the Earth-Moon center of mass, at 30 days, for two different βs.

The Dispersion of Particles in the Z-Direction for One Year

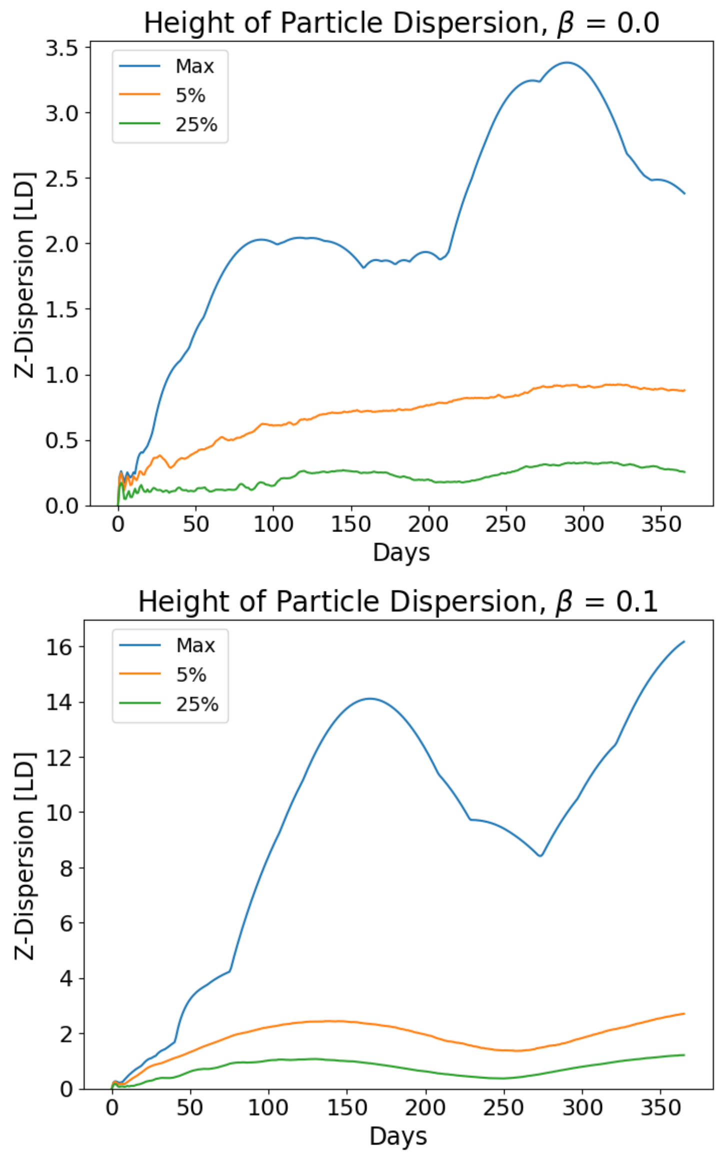

Figure 4.4: The maximum z-distance, normal to the Earth's orbital plane, between any two particles during one year of the simulations, for two different βs. As before, the blue line represents the z-distance between the two furthest particles, the orange line is the z-distance between the two furthest particles if 5% of the particles at either extreme are excluded, and the green excludes 25% of the particles at either end.

in total collide with the Earth, far more than the 21 in the original simulations. Almost no $\beta = 0.1$ particles remain orbiting the Earth or the Moon one year in, with just 62 found within the Earth-Moon hill sphere. Instead, these smaller particles are on heliocentric orbits, as seen in Figure 4.5, trailing far beyond the Earth and spreading radially outward. It should be noted that although the semi-major axis of these particles is changed, their orbits will still return through their release points and therefore this stream will still be intersecting the Earth's heliocentric orbit.

As expected from these results, the particle kernel density estimations calculated at the Earth-Moon Lagrange points are also impacted by the introduction of radiation forces. Figure 4.6 shows the L2 Lagrange point initially peaks higher than L1 for the $\beta = 0.1$ particles. This is supported by Figure 4.1, as the particles are initially drifting away from the Sun, rather than getting captured by the Earth. However, this is likely just due to the orientation of the Earth-Moon system with respect to the Sun at the time of release, and the opposite could be seen for different release times. Due to the radiation forces quickly clearing out the cis-lunar environment, more significant decreases are seen over time for the L1 and L2 points. The remaining three Lagrange points actually see more activity for the $\beta = 0.1$ particles, with peaks seen more frequently and sooner. By the end of one year, all 5 points seem to reach comparable density values, much lower than what L1 and L2 experience after one year with no radiation forces.

As we can see, radiation forces can significantly alter the short and long-term behavior of particles released from the Moon. These results do not support findings from Slíz-Balogh et al. [38], in which they presented results that showed gravitational forces dominate for particles greater than 1 μm. They concluded that radiation forces do not need to be included for short-term simulations, which we find to be incorrect. Nonetheless, it must be recalled that both the $\beta = 0.0$ and $\beta = 0.1$ simulations reflect real behaviour, as larger particles, which would be ejected during some lunar operations (as well as natural cratering events), would have an effective beta of nearly zero, at least for the purposes of these calculations. Future related work, such as those discussed in Section 4.4, is advised to include radiation forces representative of a range of dust/meteoroid sizes and properties.

XY Particle Distribution in the Heliocentric Frame after One Year

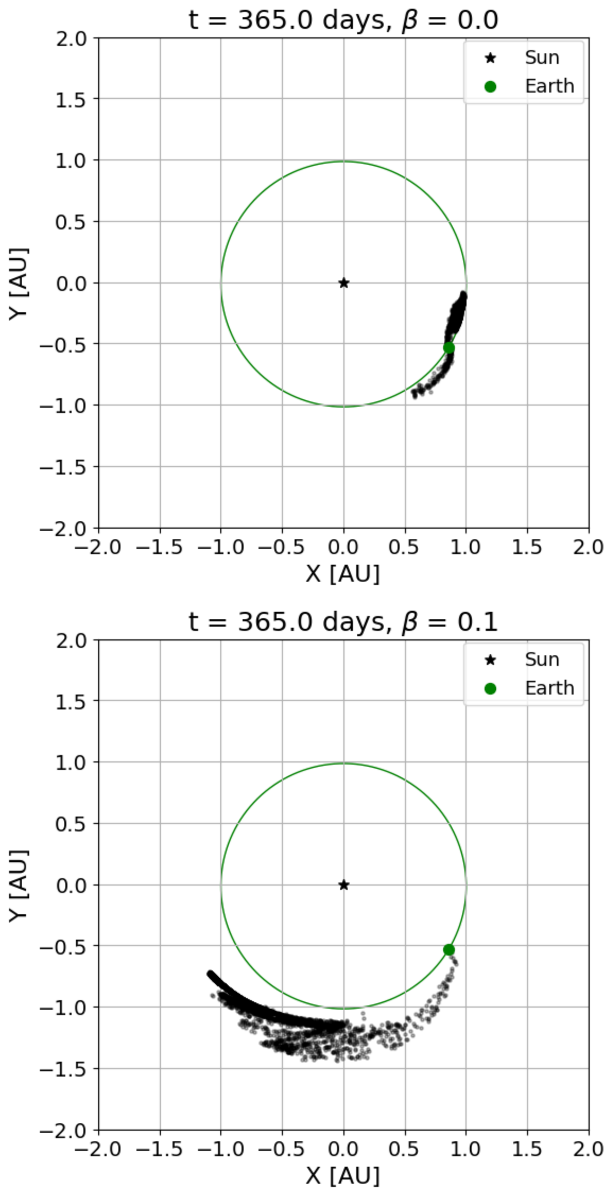

Figure 4.5: The xy-positions of the debris particles, the Earth, and the Sun, in the heliocentric frame, one year after the particles were released, for two different βs.

All 5 Lagrange Point Kernel Density Estimations for One Year

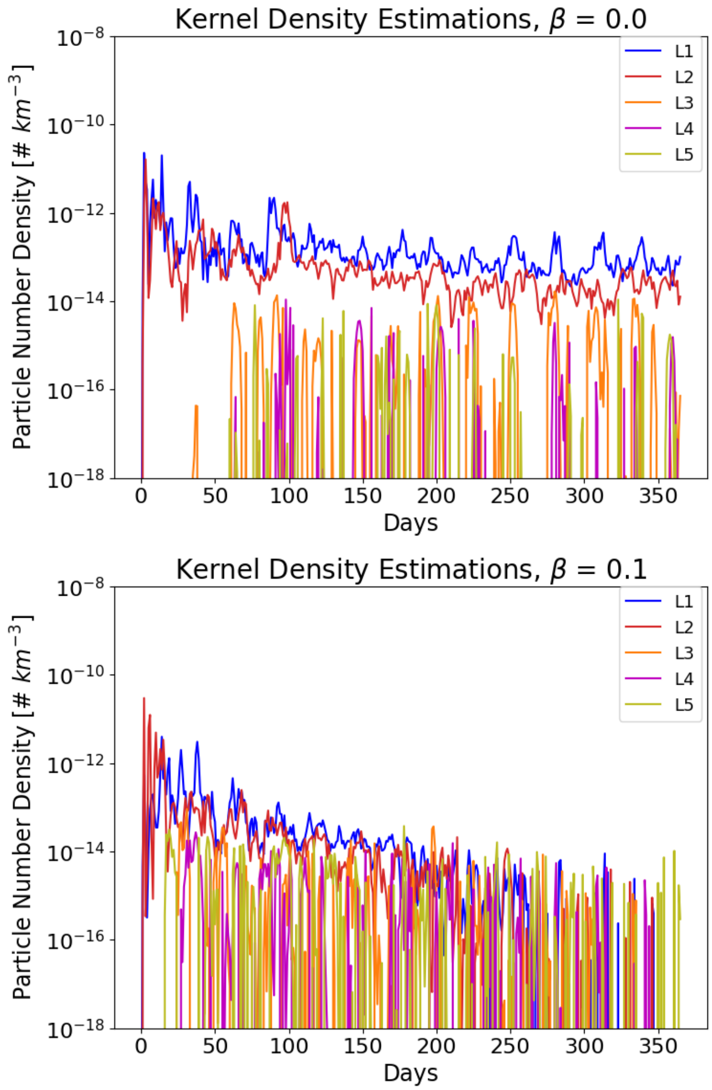

Figure 4.6: The kernel density estimations for all five of the Earth-Moon Lagrange points during one year of the simulations, for two different βs.

4.3 Sky Brightness

Polar projections of the particles across the sky of an Earth based observer show that at least some particles would be visible above the horizon every night. Large differences are seen in the distribution of the particles on the sky, as well as the incoming flux. Differences of over 6 orders of magnitude are seen at times, with these differences largely driven by the varying distances from the Earth to the particles. A large streak of particles can occasionally be seen stretching from one edge of the sky to another. Depending on the time of year and latitude of the observer, these particles can also appear just above the horizon along most of the sky. During these times, the particles may be less visible due to any neighbouring geography or city light pollution

Similar to the kernel density estimations, the brightness values calculated here can be scaled by the number of actual particles assumed to be represented by one simulation particle. The flux would scale linearly as it depends on the cross-sectional surface area of the actual particles, which is just the cross-section of one particle multiplied by the number of particles. As a reminder, the size of the simulated particles is arbitrarily assumed for the flux calculations in this study. However, as shown in the previous sections, future studies should be performed with appropriate radiations levels. As a result, given a particle's beta value, one can then estimate the actual particle size, for a given particle mass density.

Additionally, the flux values presented in this study are bolometric estimations, or the flux of sunlight across the full solar spectrum. Although the solar spectrum peaks in the visible wavelength, radiation is still produced in the ultraviolet and infra-red portions of the spectrum. As such, more detailed calculations should be converted from the bolometric flux to visible flux estimations, in order to understand the potential brightness values for the human eye. In addition, atmospheric corrections may be necessary.

4.4 Future Work

Certain aspects of this study were intentionally simplistic by design to allow for a more generalized approach, and several changes could be made to investigate more specific topics. For example, the particle release model could be adjusted to simulate individual events such as spaceship landings and takeoffs, as well as meteoroid, cometary, or anthropogenic impact events. As further plans for the eventual sustained return to the Moon become more clear, surface disruptions such as mining or construction operations could also be studied in greater detail.

Using realistic release models will also allow for improvements in making predictions for actual particle densities in cis-lunar space and corresponding sky brightness. Depending on the type of material and how it is released, estimations of the particle size distributions, as well as the albedo and phase functions, could also be determined and used to create better estimations of the brightness of the reflected sunlight. As shown previously, radiation forces impact the results of these simulations, so along with the particle sizes, estimations of the particle density could allow for radiation forces to be accurately included. Additionally, if the size and density of the particles are known, the kernel could be used to estimate the mass density of particles at locations of interest. With these more realistic assumptions, values from the brightness and density estimates could be used to determine the amount of material that could create disturbances. Examples of this include the amount of material that would generate a certain brightness, or what density/flux values become dangerous to orbiting spacecraft.

While the accuracy of these simulations was sufficient for the depth of analysis attempted here, it must be understood that these simulations are still incomplete models and greater detail could always be included. Currently the large bodies are modeled to be point sources, but asymmetric mass distributions for the Earth and the Moon create non-trivial perturbations on objects in cis-lunar space. The J2 and J4 perturbations can be included with REBOUND and REBOUNDx, but likely would only be necessary for highly detailed, longer-term simulations. Additionally, electrostatic surface phenomena that can transport material above the surface of the Moon could impact the trajectory of particles.

The kernel used to study the density of material at the Lagrange points could also be used to study a variety of different orbits and positions. One type of orbit that would be of great interest to look at is the NRHO family of orbits that will be occupied by NASA's CAPSTONE and Gateway missions. The kernel could calculate the estimated density or flux of material at any given point in the orbits. This would provide insight about if debris could ever cross trajectories with objects in these orbits, and if so, what the risk to the spacecraft or station might be. Other orbits that would be worth investigating include high-Earth orbits such as geostationary (GEO) and the orbits of important space telescopes beyond GEO like TESS and Chandra. The Earth-Sun L2 Lagrange point, which is home to the recently launched JWST, is likely safe from this material based on visual observation of Figure 3.9, although it could be worth including just for a safety check.

Chapter 5

Conclusion

Debris particles ejected from the lunar surface with enough velocity to escape the Moon's hill sphere can remain in orbit for at least a year, although most are found in orbit about the Earth rather than the Moon. A large number of particles are able escape the gravity of both, extending out into heliocentric orbits. The majority of the initially released particles do not survive a full year, with three out of four colliding with the Moon (and occasionally the Earth). Little dispersion is observed normal to the Earth's orbital plane, as most particles remain within a lunar distance. The L1 and L2 Earth-Moon Lagrange points see a large influx of material within the first few days of the simulations, and although the number density of the particles falls off, a constant presence remains throughout. After several months, L1 appears to have slightly higher density values recorded than L2, while L3, L4, and L5 begin to see sporadic particles passing through. Occasionally these three points reach comparable densities to the other two, but a sustained presence is never seen, indicating no mechanisms discovered for feeding these points, in particular the Kordylewski clouds located at L4 and L5. Additionally, radiation forces can have a significant impact on the behavior of the ejected particles.

The particles that avoid collisions are visible above the horizon for an Earth based observer almost every night of the simulations. At times these particles can create a large stream extending across the sky, while other times a ring will form around the horizon, potentially obscured from the observer. While the necessary assumptions that were made for this study strongly influence the density and brightness values reported, insight can be gathered from the results, and the techniques can be applied in the future to a number of specific problems.

As we return to the Moon, we must be careful to act sustainably in order to avoid any potential harmful consequences to our actions. While we may not be able to completely avoid producing any lunar ejecta on escape trajectories, understanding the behavior of such material can help motivate policies to limit long-lasting or otherwise disruptive debris. Although lunar dust is still a principal limiting factor in returning to the lunar surface, its challenges can eventually be overcome by using best practices in the system designs [14, 42].

Bibliography

[1] O. E. Berg, H. Wolf, and J. Rhee. 2.2.4 Lunar Soil Movement Registered by the Apollo 17 Cosmic Dust Experiment. *International Astronomical Union Colloquium*, 31:233–237, 1976. doi:10.1017/s0252921100051757. → page 7

[2] L. M. Bhalla, H. W. Hsu, R. L. Stark, and F. B. Tatom. Lunar dust/debris hazards associated with the manned flying system. *NASA CR-61106 Contract Grant: NAS8-20082*, 1965. URL https://ntrs.nasa.gov/citations/19660001414. → page 7

[3] T. H. Bird, M. I. Smokler, and D. L. Smyth. *Surveyor VI Mission Report: Part III. Television Data*. NASA JPL Technical Report 32-1262, 1968. → page 4

[4] H. Bondi. Thomas Gold. 22 May 1920 — 22 June 2004. *Biographical Memoirs of Fellows of the Royal Society*, 52:117–135, 2006. doi:10.1098/rsbm.2006.0009. → pages 3, 5

[5] J. A. Burns, P. L. Lamy, and S. Soter. Radiation forces on small particles in the solar system. *Icarus*, 40(1):1–48, 1979. doi:10.1016/0019-1035(79)90050-2. → page 15

[6] B. Chertok. *Rockets and People Volume III: Hot Days of the Cold War*. The NASA History Series, 2009. → page 2

[7] B. Chertok. *Rockets and People Volume IV: The Moon Race*. The NASA History Series, 2011. → page 7

[8] R. Christoffersen, J. R. Lindsay, S. K. Noble, M. A. B. Meador, J. Kosmo, J. A. Lawrence, L. B. Brostoff, A. Young, and T. R. Mccue. Lunar Dust Effects on Spacesuit Systems: Insights from the Apollo Spacesuits. *NASA/TP-2008-000000*, 2008. URL https://ntrs.nasa.gov/citations/20090015239. → page 8

[9] CNSA and Roscosmos. International Lunar Research Station (ILRS) Guide for Partnership, 2021. URL http://www.cnsa.gov.cn/english/n6465652/n6465653/c6812150/content.html. → pages 1, 2, 9

[10] J. E. Colwell, S. Batiste, M. Horányi, S. Robertson, and S. Sture. Lunar surface: Dust dynamics and regolith mechanics. *Reviews of Geophysics*, 45 (2), 2007. doi:10.1029/2005rg000184. → page 12

[11] D. Davis, S. Bhatt, K. Howell, J. Jang, R. Whitley, F. Clark, D. Guzzetti, E. Zimovan, and G. Barton. ORBIT MAINTENANCE AND NAVIGATION OF HUMAN SPACECRAFT AT CISLUNAR NEAR RECTILINEAR HALO ORBITS. In *27th AAS/AIAA Space Flight Mechanics Meeting, San Antonio, Texas, February 5-9*, 2017. → page 10

[12] J. R. Gaier. The Effects of Lunar Dust on EVA Systems During the Apollo Missions. *NASA/TM-2005-213610*, 2005. URL https://ntrs.nasa.gov/citations/20050160460. → pages 7, 8

[13] J. R. Gaier. Lunar Dust 101. *Lunar Dust Filtration and Separations Workshop (Cleveland, OH)*, 2008. URL https://ntrs.nasa.gov/citations/20090004550. → page 8

[14] J. R. Gaier, S. Vangen, R. Mugnuolo, S. Pirrotta, M. Bedirian, D. Lefebvre, M. Picard, T. Tomlinson, M. Wander, H. Wong, and et al. International Space Exploration Coordination Group Assessment of technology gaps for dust mitigation for the global exploration roadmap. *AIAA SPACE 2016*, 2016. doi:10.2514/6.2016-5423. → page 50

[15] T. Gold. The lunar surface. *Monthly Notices of the Royal Astronomical Society*, 115(6):585–604, December 1955. doi:10.1093/mnras/115.6.585. → pages 3, 4

[16] W. K. Hartmann. Lunar surface scientific experiments and emplaced station science. *NASA-CR-110200*, 1970. URL https://ntrs.nasa.gov/citations/19700019444. → page 8

[17] L. R. Hogan and et al. Orbiting Lunar Station phase A feasibility and definition study. Volume 1 - OLS objectives Final report. *NASA-CR-115015 SD-71-207-VOL-1*, 1971. URL https://ntrs.nasa.gov/citations/19710016356. → page 8

[18] J. T. James and N. Kahn-Mayberry. Chapter 13: Risk of Adverse Health Effects from Lunar Dust Exposure. *Human Health and Performance Risks of Space Exploration Missions*, 2009. URL https://humanresearchroadmap.nasa.gov/evidence/reports/EvidenceBook.pdf. → page 8

[19] R. M. C. Jr. Explosives and the lunar environment. *NASA, WASHINGTON PROC. OF THE 7TH ANN. WORKING GROUP ON EXTRATERREST. RESOURCES 1970*, 1970. URL https://ntrs.nasa.gov/citations/19700029974. → page 8

[20] J. E. Lane, P. T. Metzger, and C. D. Immer. Lagrangian trajectory modeling of lunar dust particles. *11th Biennial ASCE Aerospace Division International Conference on Engineering, Construction and Operations in Challenging Environments (Long Beach, CA)*, 2008. doi:10.1061/40988(323)3. → page 12

[21] D. E. Lee. White Paper: Gateway Destination Orbit Model: A Continuous 15 Year NRHO Reference Trajectory. *NASA JSC-E-DAA-TN72594*, 2019. URL https://ntrs.nasa.gov/citations/20190030294. → page 11

[22] J. M. Logsdon. *After Apollo? Richard Nixon and the American Space Program*. Palgrave Macmillan, 2016. → page 8

[23] D. R. Lord. Space Station Program Plans. *NASA-TM-X-67051*, 1970. URL https://ntrs.nasa.gov/citations/19710012566. → page 8

[24] S. Maneewongvatana and D. M. Mount. Analysis of approximate nearest neighbor searching with clustered point sets. *CoRR*, cs.CG/9901013, 1999. URL https://arxiv.org/abs/cs/9901013. → page 21

[25] G. Matthews. Celestial body irradiance determination from an underfilled satellite radiometer: Application to albedo and thermal emission measurements of the moon using ceres. *Applied Optics*, 47(27):4981–4993, 2008. doi:10.1364/ao.47.004981. → page 22

[26] J. J. Monaghan. Smoothed Particle Hydrodynamics. *Annual Review of Astronomy and Astrophysics*, 30(1):543–574, 1992. doi:10.1146/annurev.aa.30.090192.002551. → page 20

[27] D. L. Murphy and R. R. Vondrak. Effects of levitated dust on astronomical observations from the lunar surface. *Lunar and Planetary Inst., Twenty-Fourth Lunar and Planetary Science Conference. Part 2: G-M*, 1993. URL https://ntrs.nasa.gov/citations/19940011960. → page 13

[28] NASA NSpC Report. Plan for Sustained Lunar Exploration and Development, 2020. URL https://www.nasa.gov/sites/default/files/atoms/files/a_sustained_lunar_presence_nspc_report4220final.pdf. → pages 1, 2, 9

[29] H. Rein and S.-F. Liu. REBOUND: An open-source multi-purpose N-body code for collisional dynamics. *Astronomy & Astrophysics*, 537, Jan 2012. doi:10.1051/0004-6361/201118085. → page 14

[30] H. Rein and D. S. Spiegel. IAS15: A fast, adaptive, high-order integrator for gravitational dynamics, accurate to machine precision over a billion orbits. *Monthly Notices of the Royal Astronomical Society*, 446(2):1424–1437, Jan 2015. doi:10.1093/mnras/stu2164. → page 15

[31] J. J. Rennilson and D. R. Criswell. Surveyor observations of Lunar Horizon-glow. *The Moon*, 10(2):121–142, 1974. doi:10.1007/bf00655715. → page 4

[32] G. Sanders, J. Kleinhenz, and D. Linne. NASA Plans for In Situ Resource Utilization (ISRU) Development, Demonstration, and Implementation. *Committee on Space Research (COSPAR) 2022 (Athens)*, 2022. URL https://ntrs.nasa.gov/citations/20220008799. → pages 11, 12

[33] M.-Z. Shao and N. Badler. *Spherical Sampling by Archimedes' Theorem*. University of Pennsylvania Department of Computer and Information Science Technical Report No.MS-CIS-96-02, Jan 1996. → page 16

[34] R. Q. Shotts. Early water mining on the moon. *NASA, WASHINGTON PROC. OF THE 7TH ANN. WORKING GROUP ON EXTRATERREST. RESOURCES 1970*, 1970. URL https://ntrs.nasa.gov/citations/19700029975. → page 8

[35] R. Q. Shotts. Gas wells on the moon. *NASA, WASHINGTON PROC. OF THE 7TH ANN. WORKING GROUP ON EXTRATERREST. RESOURCES 1970*, 1970. URL https://ntrs.nasa.gov/citations/19700029976. → page 8

[36] A. A. Sickafoose, J. E. Colwell, M. Horányi, and S. Robertson. Experimental levitation of dust grains in a plasma sheath. *Journal of Geophysical Research*, 107(A11), 2002. doi:10.1029/2002ja009347. → page 12

[37] A. A. Siddiqi. *Beyond Earth: A chronicle of deep space exploration, 1958-2016*. National Aeronautics and Space Administration, Office of Communications, NASA History Division, 2018. URL https://lccn.loc.gov/2017058675. → page 3

[38] J. Slíz-Balogh, A. Barta, and G. Horváth. Celestial mechanics and polarization optics of the Kordylewski dust cloud in the Earth–Moon Lagrange point L5 – I. Three-dimensional celestial mechanical modelling of dust cloud formation. *Monthly Notices of the Royal Astronomical Society*, 480(4):5550–5559, Sep 2018. doi:10.1093/mnras/sty2049. → page 43

[39] J. Slíz-Balogh, B. Érdi, D. Horváth, and G. Horváth. Why was the kordylewski dust cloud observed more frequently at the L5 Lagrange point than at L4? asymmetry of the particle capture at the triangular Lagrange points of the Earth-Moon system. *Icarus*, 374:114814, 2022. doi:10.1016/j.icarus.2021.114814. → page 13

[40] T. J. Stubbs, R. R. Vondrak, and W. M. Farrell. A Dynamic Fountain model for Lunar dust. *Advances in Space Research*, 37(1):59–66, 2006. doi:10.1016/j.asr.2005.04.048. → page 12

[41] D. Tamayo, H. Rein, P. Shi, and D. M. Hernandez. REBOUNDx: A library for adding conservative and dissipative forces to otherwise symplectic N-body integrations. *Monthly Notices of the Royal Astronomical Society*, 491(2):2885–2901, Jan 2020. doi:10.1093/mnras/stz2870. → page 15

[42] S. A. Wagner. The Apollo Experience Lessons Learned for Constellation Lunar Dust Management. *NASA/TP-2006-213726*, 2006. URL https://ntrs.nasa.gov/citations/20060050035. → pages 7, 8, 50

[43] J. M. West, P. R. Bell, A. J. Calio, J. W. Harris, H. H. Schmitt, S. H. Simpkinson, K. S. W, and D. C. Wiseman. *Apollo 11 Preliminary Science Report*. NASA Scientific and Technical Information Division Office of Technology Utilization, 1969. URL https://ntrs.nasa.gov/citations/19700000726. → page 5

[44] M. M. Wittal, J. R. P. III, P. T. Metzger, B. Link, J. G. Mantovani, and D. Batcheldor. The Behavior of High-Velocity Dust Generated by Lander Plumes in the Lunar Environment. *AIAA/AAS Astrodynamcis Specialist Conference (Virtual)*, 2020. URL https://ntrs.nasa.gov/citations/20205003590. → page 12

[45] K. Yang, J. Schmidt, W. Feng, and X. Liu. Distribution of dust ejected from the lunar surface into the Earth-Moon System. *Astronomy & Astrophysics*, 659, 2022. doi:10.1051/0004-6361/202140810. → page 12

[46] A. Young. *The Apollo lunar samples: Collection Analysis and Results*. Springer, 2017. doi:https://doi.org/10.1007/978-1-4614-6185-2. → page 6

[47] E. M. Zimovan-Spreen, K. C. Howell, and D. C. Davis. Near rectilinear halo orbits and nearby higher-period dynamical structures: Orbital Stability and resonance properties. *Celestial Mechanics and Dynamical Astronomy*, 132 (5), 2020. doi:10.1007/s10569-020-09968-2. → page 11